Title

Characterization of hippocampal subregional cross-frequency associations, and the effect of Deep Brain Stimulation on memory performance in Humans

Author

TCHEMODANOV, NATALIA

Publication Date

2016

Peer reviewed|Thesis/dissertation

University of California
Los Angeles

Characterization of hippocampal subregional cross-frequency associations, and the effect of Deep Brain Stimulation on memory performance in Humans

A dissertation submitted in partial satisfaction
of the requirements for the degree
Doctor of Philosophy in Biomedical Engineering

by

Natalia Tchemodanov

2016

Abstract of the Dissertation

Characterization of hippocampal subregional cross-frequency associations, and the effect of Deep Brain Stimulation on memory performance in Humans

by

Natalia Tchemodanov

Doctor of Philosophy in Biomedical Engineering

University of California, Los Angeles, 2016

Professor Itzhak Fried, Co-Chair

Professor Dario L. Ringach, Co-Chair

Deep brain stimulation (DBS) of the Medial Temporal Lobe (MTL) in humans has offered promise for improving hippocampal-dependent learning and memory, yet little is known about how it modulates the electrophysiological mechanisms associated with hippocampal communication. Here, we explore the role of theta-gamma coupling, a putative entorhinal-hippocampal organizing mechanism, in successful memory formation, while human subjects implanted with intracranial electrodes engage in hippocampal-dependent memory tasks. Our results suggest that entorhinal area DBS, previously shown to be associated with memory enhancement, also results in substantial coupling of theta and gamma oscillations within the hippocampus, suggesting a possible mechanism for stimulation related memory enhancement. Further, we address hippocampal cross-frequency dynamics during encoding and retrieval at the level of hippocampal subfields, showing that CA1 theta high-gamma coupling increases preferentially during encoding of subsequently recollected objects, while both CA1 and CA2-3-DG exhibit memory specific cross-frequency coupling changes during retrieval. Finally, we perform a multi-task analysis to assess how generalizable is the effect of DBS across multiple entorhinal stimulation targets, memory modalities, and stimulation protocols; our results show that stimulation of entorhinal white matter enhances declarative memory encoding.

The dissertation of Natalia Tchemodanov is approved.

Mark Cohen

Wentai Liu

Dario L. Ringach, Committee Co-Chair

Itzhak Fried, Committee Co-Chair

University of California, Los Angeles

2016

To my family, who has always been a constant source of inspiration, support, encouragement and love.

Table of Contents

List of Figures

List of Tables

Acknowledgments

This work would not have been possible without contributions, help and support from many people.

Chapter 3 contains unpublished results from a task for which data has been previously published by Suthana et al., 2012. In this work, Suthana N., has designed the task, collected the data. Tchemodanov N., and Hardy, N. performed electrophysiological analysis and statistics; Principal Investigator: Fried I. Some of these unpublished results were presented at the Society for Neuroscience conference in 2012. Support for this project was possible through grants from the National Institutes of Health (5T32NS07449), the National Institute of Neurological Disorders and Stroke (NS033221), Dana Foundation, and the NIH (UCLA Neuroimaging Training Fellowship, grant number T90DA022768). This study is currently in preparation for publication.

Chapter 2 contains unpublished work, though a subset of the results has been presented at the Society for Neuroscience conference in 2015. In this work, Tchemodanov, N. designed task, collected the data, performed analysis, and wrote the manuscript. Titiz, A. collected data; Mankin E. collected data and facilitated code pipeline infrastructure; Tran, M. performed fMRI segmentation analysis; Fried I. provided human neurophysiology subject pool,lab infrastructure, funding; Suthana N., was Principal Investigator. Supported by DARPA Restoring Active Memory program (Agreement number: N66001-14-2-4029), and the NIH (Award Number: 3T32NS058280-09S1)

Chapter 4 contains unpublished data that is currently under review in *Nature Medicine*. This analysis was a collaborative undertaking that pooled data from many projects in the lab, and hence is a product of shared first authorship. In this work, Titiz A., Tchemodanov., N, and Suthana, N. designed tasks; Titiz A., Tchemodanov, N., Mankin, E., Suthana, N., collected data; Eliashiv, D., Stern, J., and Weiss, S. provided neurologist oversight during stimulation sessions; Tran, M., Kirsch D., and Schuette, P., performed fMRI segmentations; Mankin, M. authored behavior analysis codes and preprocessing pipeline; Mankin,

M., Aghajan Z., Schuette, P., performed statistics; Knowlton B. consulted on behavioral analysis; Schuette, P., pooled behavioral results; Suthana, N. wrote manuscript. Principal Investigators: Fried, I. and Suthana, N. Study was supported by grants from the National Institute of Neurological Disorders and Stroke (NS084017), DARPA Restoring Active Memory program (Agreement number: N66001-14-2-4029), and the NIH (Award Number: 3T32NS058280-09S1).

Vita

2008 BSc Neuroscience, University of California, Santa Cruz, Santa Cruz, CA

Publications and Presentations

Nanthia Suthana, Natalia Tchemanodov, Nicholas Hardy, Barbara Knowlton, and Itzhak Fried, "Deep brain stimulation increases hippocampal theta-gamma coupling ", *In Prep.*

Tchemodanov, N., Titiz, A., Mankin, E., Tran, M., Fried, I.,Suthana, N. "Memory related theta-gamma coupling in human hippocampal CA1 subfield increases during learning of subsequently recollected items". *In Prep.*

P. Schuette*, M. Tran*, A. Titiz*, N. Tchemodanov*, E. Mankin*, Z. Aghajan, D. Eliashiv, J. Stern, D. Kirsch, B. Knowlton, I. Fried, and N. Suthana.*Equal contribution., "Stimulation of entorhinal white matter enhances declarative memory encoding." *In Review.*

Titiz, A, Hill M., Eliashiv, D., Tchemodanov, N. Maoz, U., Stern, J., Tran, M., Mankin, E., Behnke, E., Suthana, N.A., Fried, I. "Theta-Burst Microstimulation in the Human Entorhinal Area Improves memory". *In Review.*

Suthana, N., Tchemodanov, N., Knowlton, B., and Fried, I."Deep brain stimulation of human entorhinal area increases hippocampal theta-gamma coupling.", *Society for Neuroscience Abstract*, October 2012

Tchemodanov, N, Titiz, A, Mankin E, Fried I, Suthana NA. "Memory related theta gamma coupling in human hippocampal CA1 subfield.", *Society for Neuroscience Abstract*, November 2015

N. Tchemodanov, T. Gazit, HG. Yamin , G. Raz , G. Jackont, F. Charles, M. Cavazza, T. Hendler, I. Fried. "Volitional control of Amygdala gamma band activity from depth electrodes in human subjects – a case study." *Society for Applied Neuroscience*, October 2016

N. Tchemodanov, S. Wang, M. Eberle, W. Liu. "A Biological Testing Platform for Data Telemetry".*associated project poster at the Biomimetic Microelectronic Systems University of Southern California ERC site visit*, June 2009

CHAPTER 1

Introduction

1.1 Motivation

Deep brain stimulation (DBS) of the Medial Temporal Lobe (MTL) in humans has offered promise for improving hippocampal-dependent learning and memory, yet little is known about how stimulation of different targets in the MTL affects memory, as well how this stimulation modulates the electrophysiological mechanisms associated with hippocampal communication as well as successful encoding and retrieval.

In the current work, we explore the role of theta-gamma coupling, a putative entorhinal-hippocampal organizing mechanism, in successful memory encoding and retrieval, while human subjects implanted with intracranial electrodes engage in a hippocampal-dependent memory task. Additionally, we assess the effect of DBS delivered to the entorhinal area on hippocampal theta-gamma coupling mechanisms. Finally, we perform a comprehensive multi-task analysis to assess how generalizable is the effect of DBS across multiple entorhinal stimulation targets, memory modalities, and stimulation protocols.

1.1.1 Cross-frequency coupling during encoding and retrieval

Decades of research have implicated the hippocampus and associated structures in the medial temporal lobe (MTL) as central to mediating the processes which support memory encoding and retrieval [1, 2]. Communication between various subfields in the hippocampus, as well as with the entorhinal cortex are thought to support this function by forming neural ensembles that represent objects in memory, and by mediating their selective reac-

tivation during retrieval. An important research topic that remains open is the search for a candidate mechanism that could be suited for such an organizational role. The coupling of gamma power (30-125 Hz) to the phase of the theta band (3-8 Hz), known as theta-gamma cross-frequency coupling has emerged as a potential organizing mechanism facilitating hippocampal-entorhinal communication; Recent evidence suggests hippocampal subfields and the entorhinal cortex may communicate via theta-gamma coupling in a complex way to support successful encoding and retrieval of memories [3–7].

1.1.2 Perturbing the circuit: electrical stimulation of the hippocampal-entorhinal network

Recently, Deep Brain Stimulation (DBS) of the MTL has been explored as a mechanism for potentiating neural correlates of learning and memory. Animal studies suggest that targeted stimulation of the entorhinal area may result in improved entorhinal-hippocampal communication, as well as in an enhancement of various processes traditionally associated with successful learning and memory [8–13]. Recently, stimulation of the human Entorhinal area was reported to enhance spatial learning [14], though what exactly was the neurophysiological effect of this stimulation on the hippocampual-entorhinal system remains an open question.

1.2 Outline of thesis topics.

In Chapter 2 of this thesis, we address hippocampal cross-frequency dynamics during encoding and retrieval at the level of individual subfields, as patients perform a hippocampally-driven object recognition task. Briefly, we will show that CA1 theta gamma coupling increases preferentially during encoding of subsequently recollected objects, as well examine evidence of memory specific CA1 and CA2-3-DG cross-frequency coupling changes during retrieval.

In Chapter 3 we will leverage the finding published earlier in our lab [14], which showed a

memory benefit for locations learned during deep brain stimulation (DBS) of the entorhinal white matter area compared to locations learned without stimulation. Here, we look at electrophysiological effects of entorhinal area stimulation; our results suggest that DBS of the human entorhinal area that enhances memory also results in substantial coupling of theta and gamma oscillations within the hippocampus, suggesting a possible neurophysiological mechanism for stimulation related memory enhancement.

In Chapter 4 we will focus on generalizing the behavioral correlates of DBS administered to the human entorhinal area, by pooling data from multiple hippocampal-dependent memory studies in which entorhinal DBS was administered with a variety of stimulation protocols, as well as to electrode targets localized *post hoc* to either white or grey matter locations of the entorhinal area. Briefly we show that stimulation of entorhinal white matter enhances declarative memory encoding, an effect that is robust across all of the other factors under consideration.

Together, this work aims to investigate the memory-supporting role of theta-gamma coupling in individual human hippocampal subfields, as well as assess whether this mechanism is readily modulated by entorhinal deep brain stimulation. A long-term goal of this work is to develop a closed-loop system for using entorhinal stimulation to improve memory performance by responding in real time to brain states related to memory. This requires identifying a neural mechanism that is relevant to memory performance and that also can be modulated by entorhinal stimulation. This work presents a first step towards this overarching goal.

CHAPTER 2

Hippocampal subregional cross-frequency coupling during encoding and retrieval

2.1 Introduction

In this chapter we will explore the role of cross-frequency (theta-gamma) coupling in encoding and retrieval processes. Hippocampal subfields are thought to support episodic memory by forming neural ensembles that represent objects in memory, and by mediating their selective reactivation during retrieval. Interactions between hippocampal subfields are crucial to orchestrate this process. The coupling between theta phase and amplitude of gamma has emerged as a potential mechanism that may play this organizational role: recent evidence suggests hippocampal subfields may communicate via theta-gamma coupling in a complex way to support memory [5–7, 15]. In particular, literature suggests that theta coupled to the lower band of gamma (30 - 50Hz) may be specifically activated at retrieval; This is supported by recordings from the human medial temporal lobe, as well as rodent CA3 and CA1 region during the stages of memory tasks when successful memory retrieval was thought to occur [5, 6, 16]. The slow gamma oscillations in the CA3 region, and in particular CA3 —CA1 synchronization, have been shown to be central to memory retrieval processes [17, 18]. On the other hand, hippocampal theta oscillations also couple to the high gamma power band (75 - 125 Hz.) at a different preferred theta phase (as compared to the preferred phase of theta-low gamma coupling) [19], and have been shown to be associated with encoding success [20]. High-gamma oscillations in the CA1 subregion have been shown to reflect sensory input from medial entorhinal cortex (MEC), and display stronger theta-gamma coupling during

behavioral stages where sensory input is associated with memory formation [15, 21, 22]. A theory proposed by Colgin et al. suggests that CA3-driven synchronization of gamma activity in the hippocampus may be mediated by theta-low gamma coupling, and put it in a state optimal for memory retrieval, whereas MEC-CA1 input-driven theta-high gamma coupling may optimize sensory input into the hippocampus and be associated with successful memory encoding, suggesting that the coupling of theta to two different gamma bands at different phases may be a mechanism by which encoding and retrieval are functionally dissociated [4]. Human studies provide a greater opportunity to control for the onset of encoding and retrieval epochs, however no analysis of theta-gamma coupling targeting individual human hippocampal subfields has been done to date; In the current study we utilize a hippocampal-dependent Object Recognition task, with an encoding stage followed by a recognition-driven retrieval stage. This design allows to directly assess epochs when encoding and retrieval of memories of objects occurs, as well as assess memory quality. The first question we aim to address with the current study is whether theta gamma coupling is functionally dissociated during encoding and retrieval states. In particular, we hypothesize that if theta-high gamma coupling (THG) does in fact facilitate encoding and not retrieval, it will be significantly increased during encoding as compared to retrieval. Converesely, we hypothesize, that theta-low gamma coupling (TLG) will be enhanced during retrieval as compared to encoding. Secondly, we would like to address the growing evidence that theta-gamma coupling affects encoding or retrieval success in a subregion-specific way. We hypothesize that THG will be selectively enhanced in CA1 during encoding of subsequently recollected objects, while TLG coupling will be observed in both CA3 and CA1 subregions, and will be selectively enhanced during correct retrieval.

2.2 Methods

2.2.1 Subjects

Sixteen adult neurosurgery patients, implanted with 8-12 intra-cranial depth electrodes for 7-10 days for pharmacoresistant epilepsy monitoring at the UCLA Ronald Reagan Medical Center were the subjects of the study. Placement of the electrodes was determined by clinical criteria, and activity was monitored to determine feasibility of, and to target subsequent surgical resection. After data preprocessing and behavioral analysis, twelve patients remained, as 4 were eliminated from the study due to presence of epileptic discharges in the data, or floor (ceiling) performance on behavioral task. All patients provided informed consent to participate in the study, which was hitherto reviewed and approved by the Medical Institutional Review Board at UCLA.

Clinical characteristics. Prior to electrode placement patients underwent Neuropsychological testing, which included the calculation of Verbal IQ and Digit span (attention) (Wechsler Adult Intelligence Scale); Verbal Memory (long-delay free-recall portion of the California Verbal Learning Test, and the logical memory portion of the Wechsler Memory Scale); Visual Memory (30-second delayed version of the Rey-Osterrieth Complex Figure Test), and Executive Function (Trail Making Test, Part B.) [23–27]. Participant age ranged from 20-48, (mean: 30.17$\pm$9.63 SD); 7/12 participants were female, and 9/12 were right-handed. Participant neuropsychiatric scores are summarized in Table 2.5.

Seizure Activity. The electrophysiological profile of seizures varied from patient to patient. Table 2.6 details electrode locations in the subregions of the hippocampus, as well as clinically - determined seizure onset zones. We assessed the possible impact of aberrant electrophysiological activity in our by – patient analysis by eliminating trials in which epileptiform oscillatory activity was detected (trial removal occurred in 9/12 patients).

2.2.2 Electrophysiology

Electrodes. Each of the 9-12 electrodes (figure 2.1) is composed of a hollow cannula containing macro iEEG contacts along its shaft, and as a microelectrode bundle, which is fed through the cannula, and emerges from the tip of the implanted intracranial electrode. This setup allows to simultaneously record depth iEEG signal on the macro contacts, as well as localized Local Field Potentials (LFPs) and single neurons (units) from microelectrodes implanted in awake, behaving human participants. Each of 8—12 microelectrode bundles contains nine 40-μm platinum-iridium microwires (8 extracellular recording electrodes, and 1 reference), resulting in 64 – 96 microelectrode recordings localized in various deep orbito- and pre-frontal, cingulate, mediotemporal, and other regions, including individual hippocampal subfields. Microelectrode LFP and single unit recordings from electrodes localized to the hippocampus were the focus of this study.

Recording. During the study the subjects sat in bed and completed the task on a laptop computer, with each session lasting 30—60 minutes. Electrophysiological data from microelectrodes is recorded and analog filtered between 0.3Hz and 7.5kHz using a 128-channel Neuroport recording system sampled at 30kHz, (Blackrock Microsystems, Salt Lake City, UT). The Object Recognition behavioral task was presented via a custom-written MATLAB script, which utilized the psychophysics toolbox [28] to present stimuli, and send event triggers signifying button presses as well as image onsets/offsets over a serial connection to the data acquisition system to be recorded on the same clock as neural data for event-related parsing of neural data. For further details on recording methods used see [29–34].

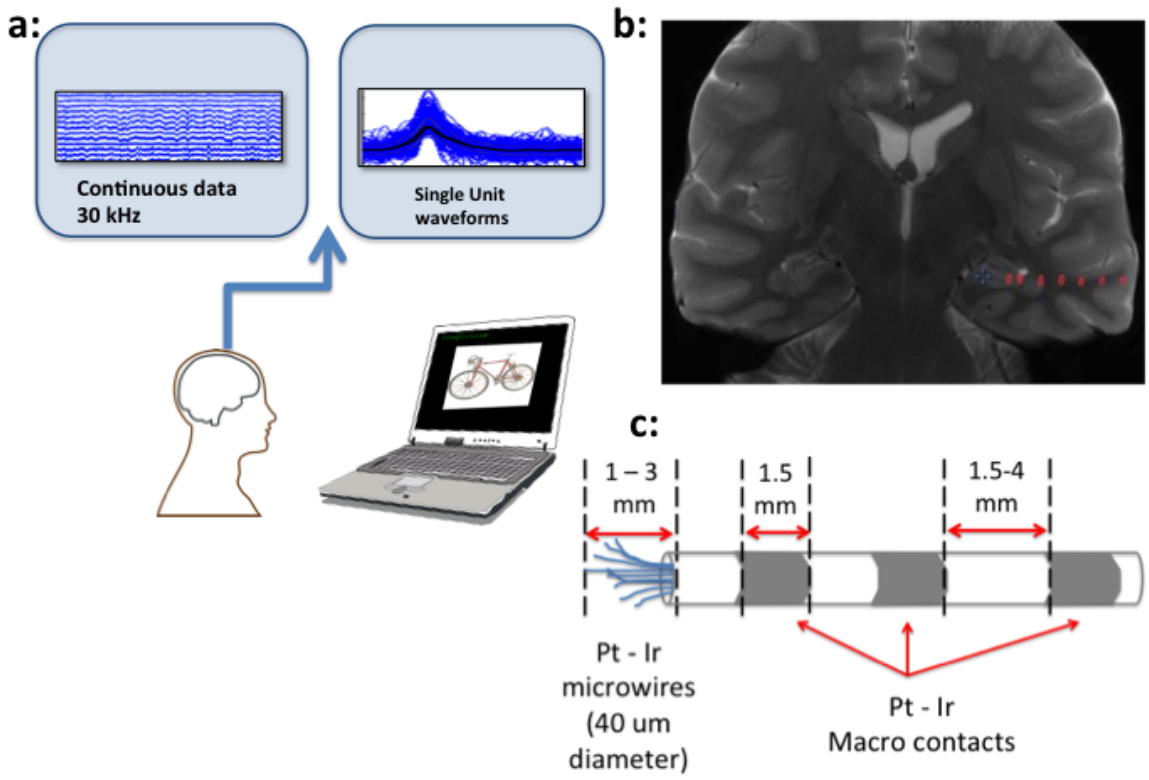

Figure 2.1: Depth electrode human neurophysiology set-up

a) micro- and macro- electrode recordings are collected from an awake, behaving human subject interacting with a behavioral paradigm via a laptop b)Example MRI showing 7-12 depth probes implanted into deep cortical regions c)A Fried-Benke probe, including 7 macro contacts along the shaft, as well as 9-lead microelectrode bundle protruding from tip.

2.2.3 Localizations

Image processing methods We utilized the BrainLab stereotactic and localization software (http://brainlab.com) [35,36], as well as FSL FLIRT (FMRIB's Linear Regression Tool) [37, 38] to co-register the post-operative high-resolution CT to the pre-operative whole brain MRI; To delineate hippocampal subfieds and other medial temporal regions, automated segmentation was performed via the ASHS [39,40] software, utilizing boundaries determined

from MRI visible landmarks correlating to underlying cellular histology [41, 42]; FSL FAST software was used to separate grey matter, white matter, and cerebrospinal fluid (CSF) [43]. Sample electrode localizations are shown in Figure 2.2.

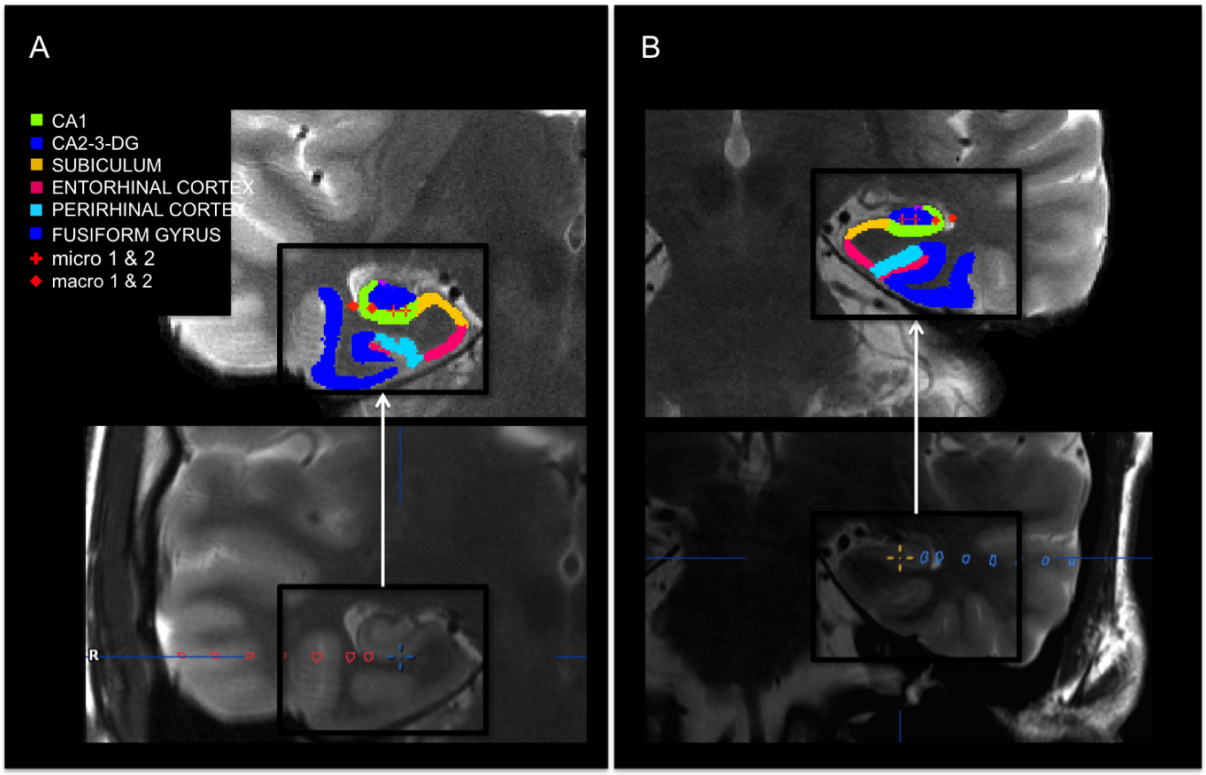

Figure 2.2: Example of microelectrode localizations to hippocampal subregions and MTL landmarks

a)Micro-electrodes (blue cross) mapped on CT scan (*bottom*) co-registered to CA1 subfield (green) mapped on high-resolution MRI (*top*). b) Analogous procedure mapping micro-electrodes (yellow cross) to CA2-3-DG combined subfield (blue).

Previously, similar methods have been used for analysis of structural or functional dissociations in subregions of the human mediotemporal lobe [44–46].

Classifications The above procedure resulted in classification of each hippocampal micro-electrode bundle as 'CA1', 'CA2/3/DG','Subiculum','Other'. 'White matter' electrodes, as well 'Subiculum' and those with 'Other' hippocampal subregion classification were excluded from further analysis.

2.2.4 Task

The task was divided into 1-6 blocks, with each block consisting of Encoding, Distractor, and Retrieval stages.

Encoding stage. A set of 30 - 50 images of objects are presented for 4 seconds. Each image is preceded by a fixation dot, which lasts for 4.5±0.5 seconds with a pseudo-randomly generated jitter period of ±0.5 sec. The patient is prompted to respond whether a specific object is larger or smaller than a shoebox, and to report their choice by pushing the appropriate button when the object appears (Figure 2.3a). The number of stimuli in the Encoding task depends on individual memory of patient, and was be altered prior to each individual block in order to make the task appropriately challenging.

Distractor stage. During the 30-second distractor task, the patient is shown a series of digits for 0.6 seconds each, and is prompted to press buttons corresponding to odd or even numbers (Figure 2.3b).

Retrieval stage. Each encoded image is associated with a lure (a different object of the same type) as well as a foil (a visually dissimilar object from a related but different category). All lures, foils and encoded images are shuffled and presented in a forced-choice quiz, which instructs the patient to assess how sure he or she is whether an image is old or new (1—Definitely new, 2—Likely new, 3—Maybe new, 4—Maybe old, 5—Likely old, 6—Definitely old) (Figure 2.3c).

The initial four subjects (444—450) completed a slightly different version of the paradigm, where they were not prompted to provide a size judgment (bigger/smaller than a shoebox) during the Encoding stage, hence for these subjects object encoding occurred in an incidental fashion.

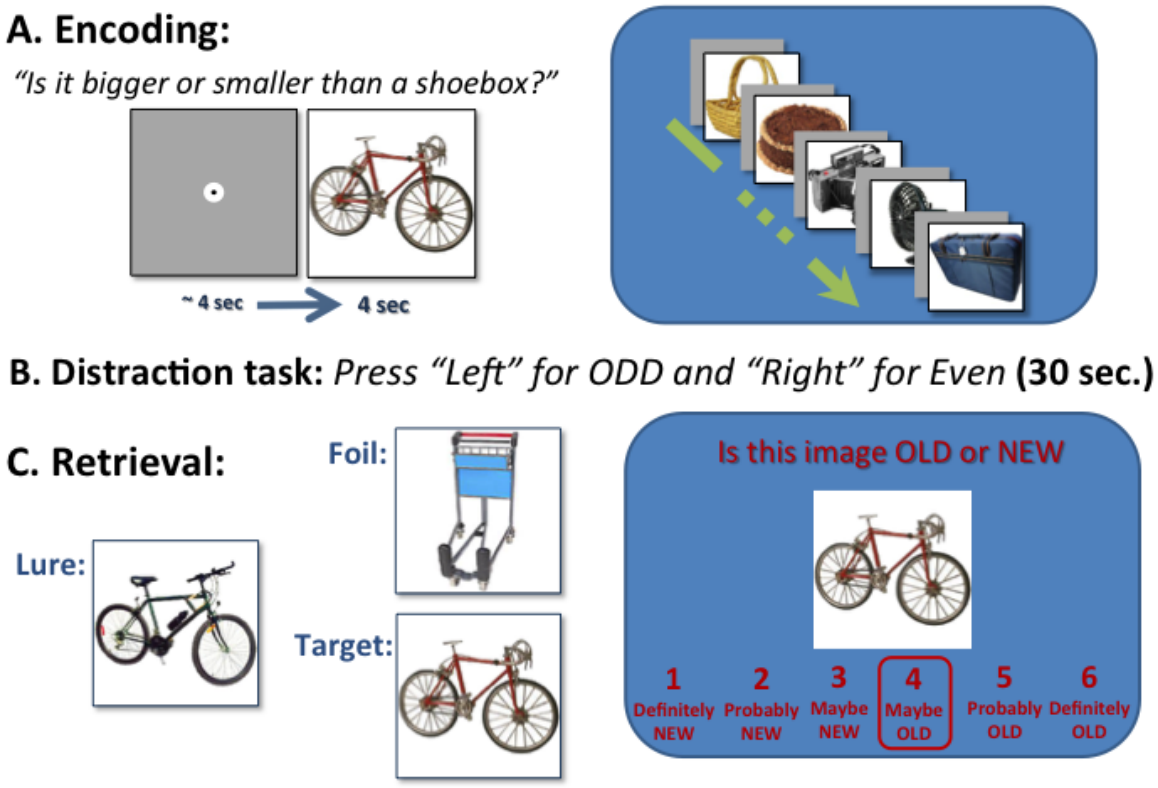

Figure 2.3: One block of the object recognition task

a) During the Encoding stage 20-50 images of objects were shown for 4 sec. b) During the Distractor stage, subjects were instructed to push the left (right) key when they see an odd (even) number. Numbers were shown for 0.6 seconds each. c) During the retrieval stage the subjects were presented all of the items present in the encoding stages as well as an equal number of both, lures (semantically similar objects), and foils (unrelated objects), which they ranked as old or new by selecting numbers 1-6.

2.2.5 Preprocessing

After data acquisition, the raw electrophysiological data was preprocessed utilizing the *Patient Data Manager*, a database and MATLAB code pipeline developed in our lab to automate data processing and parse datasets into a trial-based analysis framework.

Motion artifact rejection: Each set of 8 channels corresponding to a specific brain region is analyzed together for presence of high-amplitude artifact. Due to low trial counts we retain trials where such signal is present, however generate a masking vector that may be used to eliminate those bad regions during analysis. Any sample that is more than 6 interquartile ranges removed from the median is designated a potential artifact. Then, potential artifacts that are simultaneously detected on at least half of the leads are attributed to movement, and recorded as artifacts. The temporal locations of these artifacts are stored in a separate masking vector, which contains islands of masking values (NaNs), whose indices corresponding to location of artifacts in the continuous data signal. This masking vector can be multiplied with the continuous signal in order to remove noisy regions.

Filtering: Continuous 30 kHz data was filtered with a coarse low-pass 300Hz corner frequency least squares finite impulse response (FIR) filter consisting of 300 tabs, and decimated to a sampling rate of 1 kHz. This coarsely-filtered downsampled signal, was further high-passed at 1Hz to remove any DC drift, generating a clean lfp signal. A filter bank of bandpass signals at relevant EEG bands was generated by filtering the lfp signal through a series of least-squares FIR filters for which the filter order was computed as three times the rounded ratio between the lower frequency band and the sampling rate. Filter implementation was similar to *eegfilt.m* function in the EEGLAB toolbox [47]. EEG bands include Theta (3—8 Hz.), Alpha (9—15 Hz.), Beta (16—29 Hz.), low Gamma (30—45 Hz.), and high Gamma (75—125 Hz.). An instance of the motion artifact mask with adjustments for filter widths was created for each EEG bands. This was done in order to account for the filtering step, in which convolution of the coarse signal with a filter is expected to widen the noisy regions by the number of tabs present in the filter. In order to avoid introducing phase distortion, filtering was performed in a bidirectional manner via the *filtfilt.m* matlab function [47].

2.2.6 Behavioral analysis

For each session, the object stimuli are separated into three behavioral categories based on patient responses during Retrieval (quiz) stage. The RECOLLECTED category consists of images in which the patient correctly identified the target image, while correctly rejecting its lure. The MISSED category contains all images in which the patient made a mistake regardless of the lure, and the FAMILIAR category contains stimuli for which the patient correctly identified the target image as a previously seen image, but also incorrectly accepted the lure.

Measuring D': D' is a measurement that emerges as a result of modeling each subject's internal response (i.e,'familiarity') distribution for retrieval targets (signal), as well as retrieval lures (noise). D' measures the separation between the signal (target) and noise (lure) distribution means, compared against the standard deviation of the signal plus noise distributions. For normally distributed signal and noise distributions with mean and standard deviations μ_S, σ_S, and μ_N, σ_N respectively, D' is defined as:

$$D' = \frac{\mu_S - \mu_N}{\sqrt{\frac{1}{2}(\sigma_S^2 + \sigma_N^2)}},$$

and an estimate of D' is calculated from hit rate and false-alarm rate as: $D' = Zhitrate - Zfalsealarmrate$, where the function Zp, $p \in ([0,1]))$ is the inverse of the cumulative distribution function of the Gaussian distribution (hence it is a difference in their two $z-$scores).

We also computed the subsequent retrieval target Hit Rate for each encoding image as $Pr('yes'|target)$, as well as a *certainty* metric, obtained from button press responses during the quiz, and which took on the values of 1—(not very certain); 2—(somewhat certain), and 3—(very certain). To investigate a possible priming effect resulting from quiz lure stimuli appearing prior to target stimuli and therefore priming the memory, we computed an *isPrimed* measurement for each trial, which allowed us to assess whether order of presentation of target images and their lures may have affected performance (see 2.3.1).

2.2.7 LFP dataset construction

LFP datasets were created as follows: for each target image belonging to either 'RECOLLECTED' or 'MISSED' behavioral category, the LFP trace recorded during its encoding was placed either into the RECOLLECTED$_{enc}$ or MISSED$_{enc}$ dataset. Likewise, the LFP traces collected during the retrieval of its corresponding target and lure was placed into the RECOLLECTED$_{retr}$ or MISSED$_{retr}$) dataset. The rationale was that the same 'well-formed' memories were analyzed during encoding as the ones accessed during retrieval.

2.2.8 Computing Phase-Amplitude Coupling with the Modulation Index MI

To compute hippocampal cross-frequency coupling during recollected, or missed trials, we measured the Modulation Index (MI) between the phase component of a low-frequency (e.g. theta) band Φ_θ, and the amplitude component of a high-frequency (e.g. gamma) band $A_{\gamma high}$ during 0—4 seconds after Encoding image onset, utilizing a previously published method [48]. For example, to determine MI for N trials of the MISSED$_{enc}$ dataset, a trial-by-time matrix pre-filtered at the theta (3–8 Hz) range, $\{X_\theta[t]\}_{1:N}$, was converted into a complex-valued signal with the Hilbert transform. Note that a pad of 2 seconds was used on either side of each trial prior to the filtering as well as computing the Hilbert transform. Further, trials were truncated to time regions $[t_0 : t_{end}]$ corresponding to 0—4sec. after image onset (and hence removing the pre-filtering pad), and re-shaped into a $1 - by - N \cdot [t_{end} - t_0]$ vector of concatenated trials. Then the phase angle time series of this complex-valued signal was measured, resulting in the instantaneous phase of the low-frequency band, Φ_θ. Similarly, padded lfp trials pre-filted at the high-frequency (e.g. high-gamma) (75—125 Hz) range $\{X_{\gamma high}[t]\}_{1:N}$ were converted via the Hilbert transform to complex-valued form, and then truncated to time regions $[t_0 : t_{end}]$ and vectorized; the complex modulus (aboslute value) was used to compute the instantaneous high-frequency amplitude signal $A_{\gamma high}$. To measure strength of coupling between the theta phase Φ_θ and gamma amplitude $A_{\gamma high}$, those two signals were combined into an analytic complex-valued signal via Euler's formula, and then

the vector mean was computed, with the raw modulation index measured as the resultant vector length:

$$MI_{raw} = \sum_{t=1}^{n} |A_{\gamma high} \cdot e^{i\Phi_\theta}|, \tag{2.1}$$

while the preferred phase is measured as the resultant vector's angle.

Surrogate Analysis: potential autocorrelations in the signal were accounted for by generating 2000 surrogate Modulation Indices, $\{MI_{surr}\}_{1:2000}$, in which the amplitude component is shifted with respect to the phase component by a pseudorandomly generated lag value at least 300 msec. in duration. A normalized MI index MI_{norm} is generated by z-scoring against the normal distribution fitted to $\{MI_{surr}\}_{1:2000}$.

2.2.9 Statistical Analysis

We used Generalized Estimating Equations (GEE) [49], to model the effect of function (Encoding/Retrieval), memory condition (Recollected/Missed), and/or subregion (CA1/CA2-3-DG) on the theta-gamma coupling MI outcome variable. GEE is used to estimate parameters of a Generalizes Linear Model in a scenario where unknown correlations between observations (in our case, individual microelectrodes recorded from the same hippocampus) exist, hence allowing to investigate the relationships between clustered response data and outcome measures when the observations have been conducted via a within-subject repeated measures design.

2.3 Results

2.3.1 behavior

The mean target hit rate (rate of correctly identifying target images as OLD), was 0.74 ± 0.09, whereas false-alarm rate (rate of incorrectly identifying lure images as OLD) was 0.22 ± 0.11. We utilized the D' metric to assess recognition memory, and quantify the separation between the signal (target hits) and noise (lure false alarms) distributions. The D' indices ranged

from 0.87–2.42, ($D'_{mean} = 1.51 \pm 0.53$). Figure 2.4 depicts ROC curves for each patient's D' scores (Figure 2.7a), including the mean ROC curve, where the ordinate line indicates no sense of familiarity (chance performance). All 12 patients demonstrated ROC curves with D' scores that were well deflected from the ordinate, showing they were engaged in the task. At the floor of behavior (poor recognition), a critical $D'_{crit} = 0.68$ threshold was defined (Figure 2.7b). If the hit and false alarm distributions are modeled as gaussians with respect to some internal response variable (ie. familiarity), D'_{crit} was such that these distributions were overlapped to the extent that their point of separation is within one quartile of either mean. This resulted in elimination of one subject from the orignial 16 (already excluded from the 12 subjects undergoing analysis). At the ceiling of performance, we eliminated any subjects in which less than 8 'MISSED' trials were detected. Across the 12 subjects, the mean D' value was 1.51 ± 0.53. These results are summarized in Table 2.1

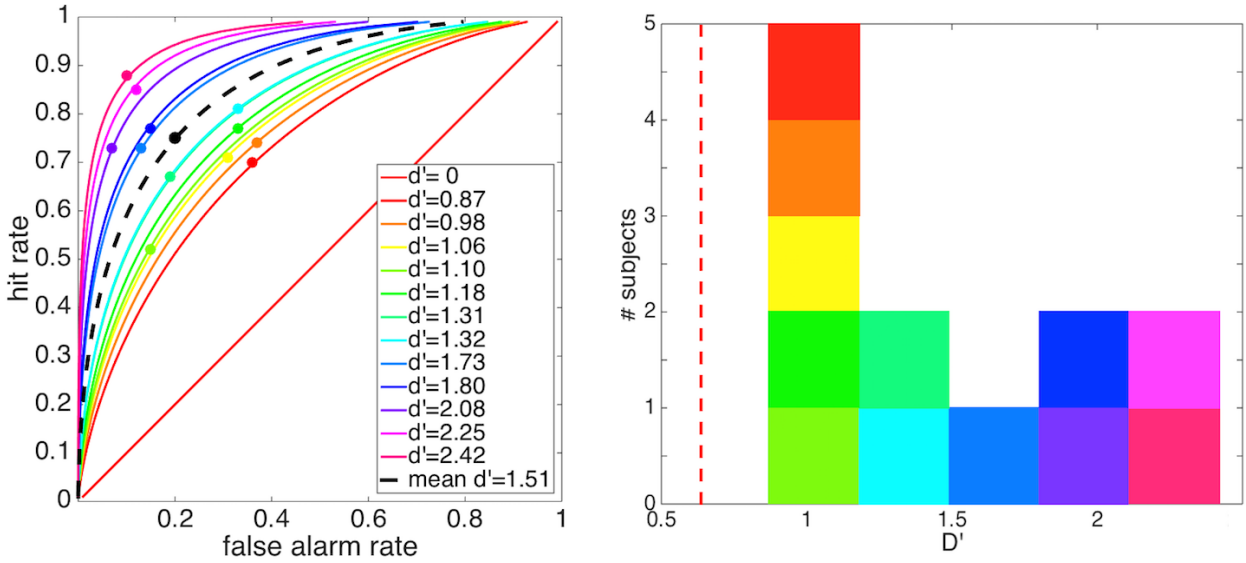

(a) ROC curves (all subjects) (b) D' score histogram

Figure 2.4: Estimated D' ROC curves and D' histogram for all subjects

a)Curves estimated from inverse of gaussian cdf of hit rate and false alarm rate. Each color represents an individual subject. Dashed curve represents mean D'. Dots plotted at actual hit and false alarm rates for each patient. b)Dashed line $D'_{crit} = 0.68$ is a critical threshold at which target and lure separation is critically impaired. Each square represents one subject, color-matched to curves in a.

We addressed the possibility that subjects may use different recognition strategies depending on whether the target or lure first appears on the quiz, which may create inherent bias during the quiz due to the order in which the target-lure images are presented (for instance, recollection strategy may differ if a lure image is presented first in the retrieval quiz, hence 'priming' the subsequently appearing target, as compared to the scenario when a target appears first). Further, this phenomenon may vary across quintiles. Effects of position quintile, and priming on D' were assessed with a 2-way repeated measures ANOVA (position quintile, priming). In contrast to [50, 51] no effects were found for priming (F=2.019, p=0.183,MS=3.57,SS=3.57), quintile (F=1.22,p=0.314,MS=1.1,SS=2.125), or for their interaction (F=0.89,p=0.445,MS=1.04,SS=2.67).

Behavioral metrics during object recognition							
Subject No.	Number of stimuli	Hit rate *(Target)*	False Alarm rate *(Lure)*	No. in memory condition *Recall*	*Miss*	*Familiar*	Dprime
444	100	0.73	0.07	68	24	4	2.08
445	80	0.74	0.38	20	21	38	0.98
447	80	0.88	0.10	51	8	18	2.42
450	116	0.77	0.33	56	27	33	1.18
452	150	0.52	0.15	62	71	16	1.10
454	190	0.7	0.36	69	57	63	0.87
456	130	0.85	0.12	99	19	12	2.25
460	200	0.77	0.15	139	46	15	1.80
461	98	0.67	0.19	56	32	10	1.31
465	250	0.73	0.13	156	67	26	1.73
466	169	0.81	0.33	86	31	51	1.32
467	149	0.71	0.31	70	43	36	1.06
Average:		0.74 ± 0.09	0.22 ± 0.11				1.51 ± 0.53

Table 2.1: Behavior

2.3.2 Prevalence of Stimulus-locked power increases

We then used our localization technique to assign hippocampal subregions to each hippocampal recording site (20 hippocampal regions total). Electrodes in 9 hippocampi (7 right and 2 left) were localized to the CA1 subregion and yielded a total of 61 microwire CA1 recording sites. Electrodes in 11 hippocampi (5 right and 6 left) were localized to the CA2-3-DG combined subregion, and yielded a total of 71 microwire recording sites.

First, the prevalence of stimulus-locked Theta (3—8hz), Low-Gamma (30—50hz), and High-Gamma (70—125hz) power increases on CA1 and CA2-3-DG electrodes independent of cross-frequency coupling was quantified for both encoding and retrieval blocks. Representative trial-locked power oscillations prevalent on encoding and retrieval electrodes are shown in Figure 2.6. The counts of electrodes demonstrating significant event-locked power oscillations or theta-gamma coupling (regardless of memory condition) were quantified separately for encoding and retrieval. The filter-hilbert method (section 2.2.5) was utilized to isolate the power time series for each electrode. For encoding, we compared mean power in the 0.3 to 1.3 second window after the onset of each encoding trial to a corresponding -2 to -1 second baseline (fixation) window. For retrieval, we compared mean power in the 0.3 to 0.7 second window after the onset of each encoding trial to a corresponding -0.750 to -0.050 second baseline (inter-trial period) window. In both cases, paired t-tests and false-discovery rate (fdr) adjustment for multiple comparisons were utilized to quantify power increases on an electrode-by-electrode basis and to count fractions of electrodes displaying significance, with ratios modeled as binomial trials (95% CIs computed with Clopper Pearson method).

Overall, the most striking trend is in the relative low counts of CA1 electrodes displaying evoked theta power increase during both encoding and retrieval (15%; 23%) as compared to CA2-3-DG electrodes (54%; 49%). Additionally, there is a significant increase in CA1 electrodes displaying high-gamma evoked power increases during encoding (30%) as compared

to retrieval (13%) (Figure 2.5, red asterisk), and the absence of this effect in CA2-3-DG electrodes(29%; 28%). Finally, chance level of electrodes display evoked power increase from baseline in the low-gamma band in both regions and both conditions(CA1:7%, 3% ; CA2-3-DG:0%, 1%).These data are summarized in figure 2.5 and table 2.2.

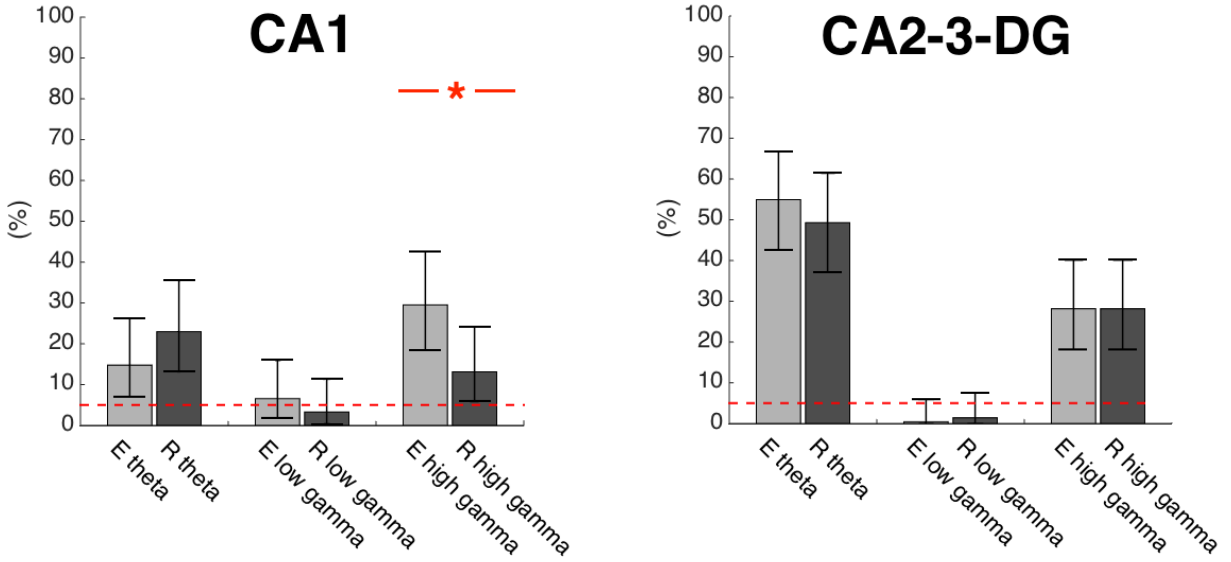

(a) % CA1 electrodes showing evoked power responses

(b) % CA2-3-DG electrodes showing evoked power responses

Figure 2.5: Percent electrodes showing significant evoked theta, low-gamma, high-gamma power increases from baseline during Encoding or Retrieval in CA1 and CA2-3-DG

Red dotted line depicts chance fraction of electrodes; counts have been fdr-corrected.

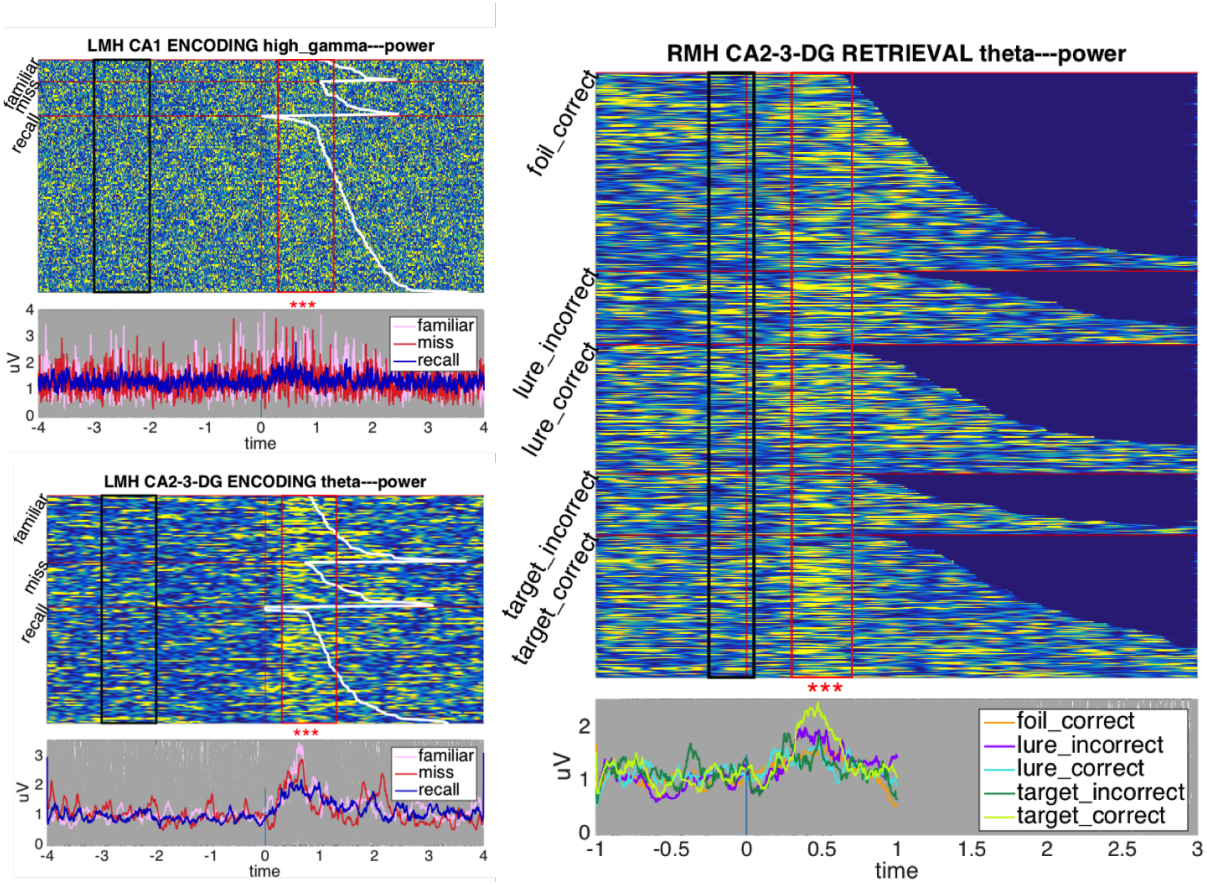

Figure 2.6: Sample electrodes showing significant evoked power increases during Encoding and Retrieval

For each plot, image onset is at $t_0 = 0$. Trials have been sorted by memory condition. Yellow color indicates increase in normalized power (arbitrary units). Bottom panels display averaged responses for each memory type. Encoding trials within each condition are shown sorted by response time (white line) to size judgement question (is object bigger/smaller than a shoebox?). Retrieval trials have been sorted by reaction time (each trial ends upon memory judgement). Red boxes depict time windows during which average power was compared to baseline period (black box)]. Asterisks show false-discovery rate (fdr) adjusted p-value

2.3.3 Prevalence of Phase-Amplitude coupling irrespective of memory

We likewise quantified CA1 and CA2/3/DG electrodes that display functionally-relevant cross-frequency coupling (figure 2.7). Briefly, we computed Theta Low-Gamma phase-

amplitude coupling (TLG cfc) and Theta High-Gamma phase-amplitude coupling (THG cfc) on all CA1 and CA2/3/DG electrodes during Encoding and Retrieval (across all stimuli) utilizing the normalized modulation index (MI_{norm}) described by Canolty et. al. (see section 3.2.5). We found that out of CA1 electrodes approximately 50% were significantly coupled in the THG cfc condition during both encoding and retrieval, as compared to approximately 25% for CA2-3-DG. Theta low-gamma coupling in CA1 was seen on 34% of electrodes during encoding, but displayed a modest increase to 52% during retrieval. Table 2.2 summarizes these data.

Note that all normalized MI index measurements (p-vals associated with z-scores) were fdr-adjusted before being considered significant. These data are summarized in and

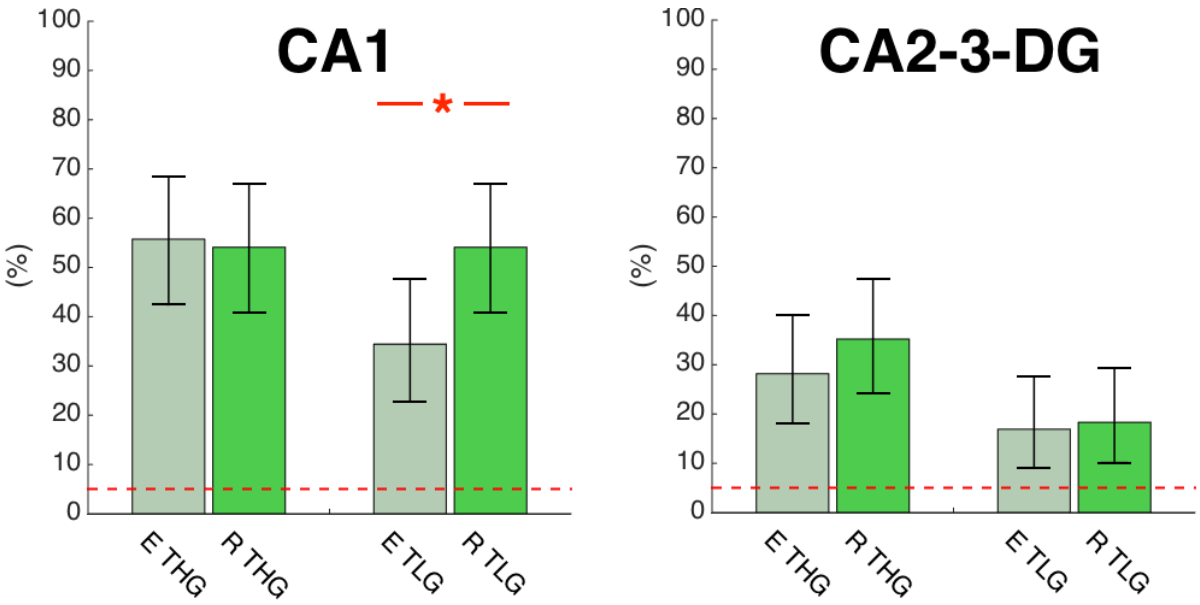

(a) % coupled CA1 electrodes (b) % coupled CA2-3-DG electrodes

Figure 2.7: Percent electrodes showing significant Theta-Gamma coupling (THG and TLG) during Encoding or Retrieval in CA1 and CA2-3-DG
red dotted line –chance fraction of electrodes; counts have been fdr-corrected

Electrode counts showing significant Power increases and Theta-Gamma Coupling during Encoding and Retrieval on electrodes localized to CA1 and CA2-3-DG								
Sub-field	No. Micros	No. Hippo-campi	No. Subj.	Encoding Power*			Encoding PAC*	
				theta	*low gamma*	*high gamma*	*TLG*	*THG*
CA1	61	9 (7 Right, 2 Left)	8	0.15 9/61el. 3/9reg.	0.07 4/61el. 2/9reg.	0.3 18/61el. 3/9reg.	0.34 21/61el. 4/9reg.	0.54 33/61el. 6/9reg.
CA2-3-DG	71	11 (5 Right, 6 Left)	9	0.55 39/71el. 6/11reg.	0.00 0/71el 0/11reg.	0.28 20/71el. 3/11reg.	0.17 12/71el. 5/11reg.	0.25 18/71el 6/11reg.
Sub-field	No. Micros	No. Hippo-campi	No. Subj.	Retrieval Power*			Retrieval PAC*	
				theta	*low gamma*	*high gamma*	*TLG*	*THG*
CA1	61	9 (7 Right, 2 Left)	8	0.23 14/61el. 3/9reg.	0.03 2/61el. 1/9reg.	0.13 8/61el. 1/9reg.	0.52 32/61el. 6/9reg.	0.54 33/61el. 7/9reg.
CA2-3-DG	71	11 (5 Right, 6 Left)	9	0.49 35/71el. 8/11reg.	0.01 1/71el. 1/11reg.	0.28 20/71el. 5/11reg.	0.15 12/71el. 5/11reg.	0.37 26/71el. 8/11reg.

Table 2.2: Prevalence of event-related power increases and theta gamma coupling (THG, TLG) on CA1 and CA2-3-DG electrodes

*fdr corrected

2.3.4 No evidence of an Encoding-Retrieval functional dissociation in theta-gamma coupling.

We sought to assess whether there is an encoding-retrieval functional dissociation between phase-amplitude coupling in CA1 and CA23DG irrespective of quality of encoded memory. We hypothesized that if, indeed, the CFC of theta with high gamma is upregulated specifically during the process of encoding, (and comparatively, the PAC of theta with low gamma is upregulated specifically during retrieval) then we would expect that electrodes displaying significant coupling during encoding would become quieted during retrieval and vice-versa. If we then plot modulation indices measured during encoding vs. retieval for each electrode, all the data points should fall well above (below) the diagonal. Instead, we saw a linear relationship (Figure 2.8) between theta gamma coupling (both TLG and THG) measured during encoding vs. retrieval, suggesting that the same electrodes that become coupled during encoding also become similarly coupled during retrieval.

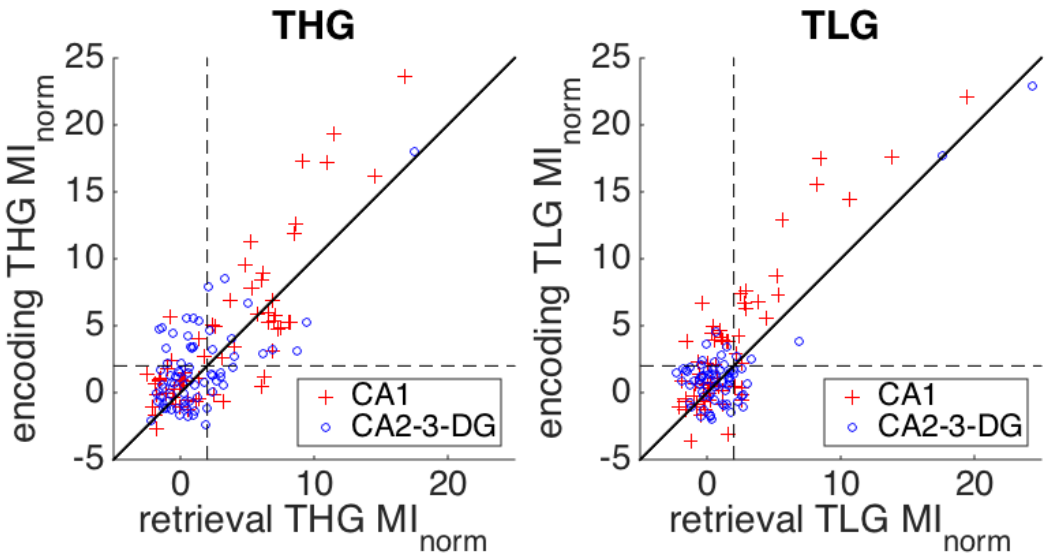

Figure 2.8: Cross-Frequency coupling during Encoding vs. Retrieval on CA1 and CA2-3-DG electrodes

Each point represents $MI_{norm,encoding}$ and $MI_{norm,retrieval}$ for one electrode. Dotted lines represent threshold of MI significance ($MI > 1.96$)

To quantify this relationship, taking into account potential correlations in data between adjacent electrodes we constructed two Generalized Estimating Equations models, with either THG or TLG as the dependent variable, the *subregion* (CA1, CA2-3-DG) and $function$ (Encoding, Retrieval) as factors, and subject ID as a within-subject variable. We hypothesized that a significance in the $subregion * function$ interaction term would provide evidence for functional dissociation between encoding and retrieval in CA1 vs. CA2-3-DG.

There was a significant main effect of subregion (CA1, CA2-3-DG) on THG coupling (B = -2.27, Std. Error = 1.05, p = 0.03), however no significance in either the 'function' factor (B = -0.267, Std. Error = 0.33, p = 0.417), or the 'subregion*function' interaction term (B = -0.244, Std. Error = 0.52,p = 0.64). This effect is not observed in the TLG model, demonstrating no significance for either main effect or their interaction. Together, this dataset suggests that while CA1 demonstrates stronger THG coupling than CA2-3-DG, neither region demonstrates significant encoding-retrieval differences in either THG or TLG, and hence provides no evidence of theta-gamma coupling-related functional dissociation during encoding and retrieval.

2.3.5 CA1 theta gamma coupling increases preferentially during encoding of subsequently recollected objects.

Electrodes identified in section 2.3.4 as displaying significant THG or TLG coupling across either Encoding or Retrieval (further called 'PAC' electrodes) were selected to investigate whether successfully encoded (retrieved) memories also demonstrate stronger Phase-Amplitude coupling. For the Encoding stage, cross-frequency coupling was separately assessed during original viewing of subsequently 'Recollected' (quiz targets correctly identified and lures correctly rejected; RECOLLECTED_{enc} dataset) and subsequently 'Missed' objects (on subsequent quiz mistake occurred on target; any response on lure; MISSED_{enc} dataset) as is described in 2.2.7– 3.2.5.

We next wanted to ask whether theta gamma coupling became stronger or more common

preferentially during successful encoding of objects. We hypothesized that on PAC electrodes localized to the CA1 subregion, THG coupling will increase during successful encoding. We addressed this question from two perspectives. First, we wanted to simply see if more CA1 electrodes became recruited for successful coupling during viewing of subsequently-recollected objects. This would indicate that THG coupling may become more common across CA1. We then looked at whether theta-gamma coupling strength changed, suggesting coupling becomes stronger locally in specific CA1 electrodes.

More CA1 electrodes recruited for coupling during encoding of subsequently recollected objects: We assessed the percentages of electrodes demonstrating significant coupling during the encoding stage of each memory condition (figure 2.9a,c), finding that in CA1 significantly more PAC electrodes displayed enhanced THG and TLG coupling during encoding of RECOLLECTED vs. MISSED trials (THG: 90.6% vs. 56.3% of total PAC electrodes; TLG: 57.1% vs. 19% of total PAC electrodes; red asterisk on figure 2.9a,c). This memory-specific effect was especially pronounced in CA1 during THG coupling, with over 90% of all PAC electrodes becoming significantly coupled during the RECOLLECTED$_{enc}$ condition. In CA2-3-DG, no significant difference was observed between the percentage of RECOLLECTED$_{enc}$ (55%) and MISSED$_{enc}$ (45%) electrodes engaged in either type of theta high-gamma coupling. For all percentages, counts were modeled as binomial trials; 95% CIs calculated via Clopper-Pearson method. Data summarized in Table 2.4.

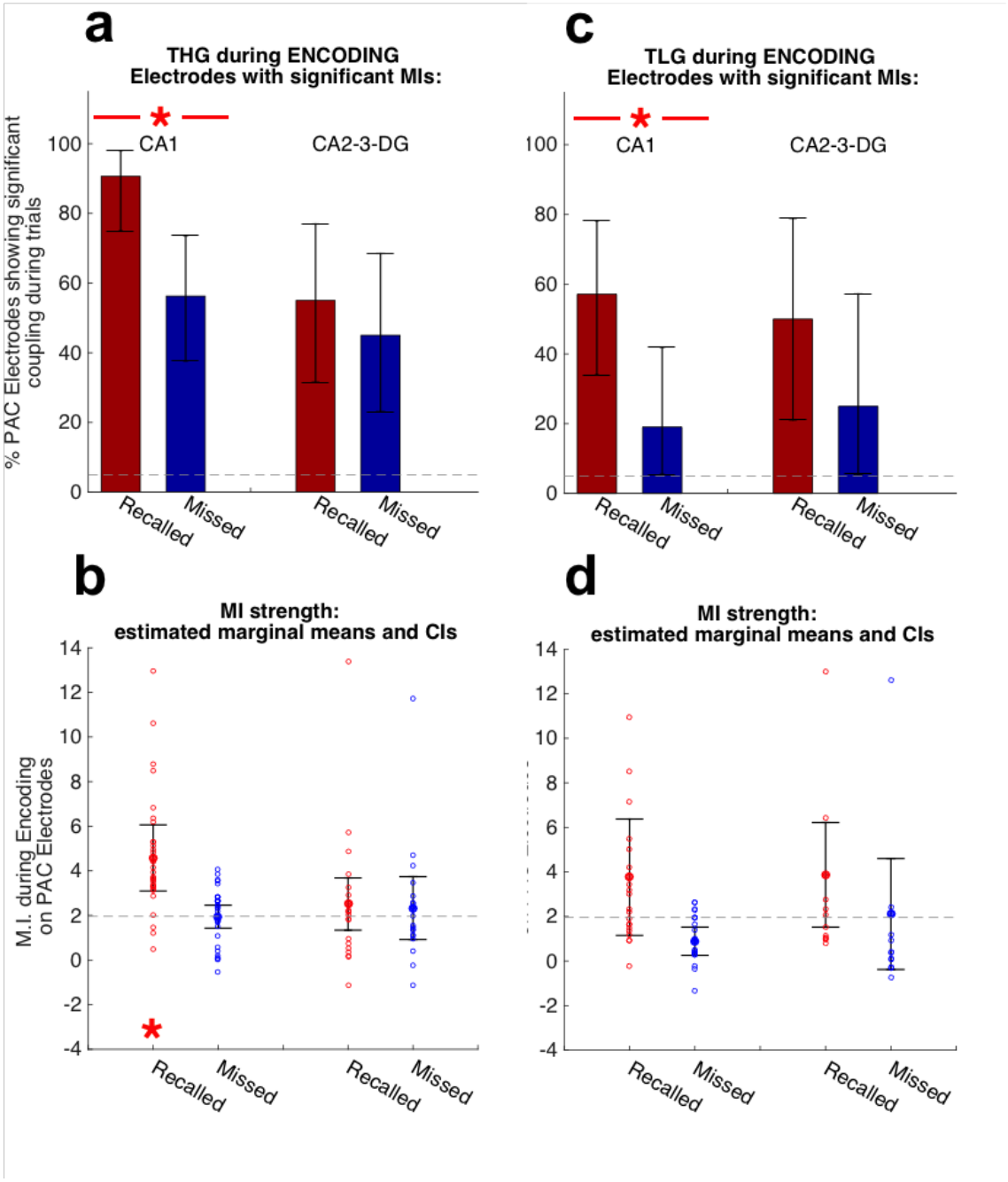

Figure 2.9: Cross-Frequency coupling in CA1 and CA2-3-DG during encoding of subsequently recollected and forgotten trials

CA1 electrodes show difference in THG coupling strength during encoding of subsequently

recollected objects: In addition to electrode ratios, we modeled the effect of memory condition and hippocampal subregion on coupling strength. We hypothesized that CA1 will show enhancements in coupling strength during the RECOLLECTED condition. Two Generalized Estimating Equations (GEE) models with either THG or TLG cross frequency coupling strength as the dependent variable, the 'subregion' (CA1, CA2-3-DG) and 'memory condition' (RECOLLECTED, MISSED) as factors, and electrodes as a within-subject variable were constructed. For the THG model we saw a significant effect in the interaction term (B= -2.45; Std. Error = 1.109; p = 0.027) indicating a region-specific difference in coupling strength between the missed and recollected conditions; The estimated marginal means, (Figure **??**b,d), and 95% CIs of the interaction term show that MI strength on CA1 electrodes during the RECOLLECTED$_{enc}$ group was significantly elevated above threshold $MI_{threshold} = 1.96$. This was not observed for the Missed group, or for either group on CA2-3-DG electrodes, suggesting a memory-specific upregulation in THG cross-frequency coupling strength specifically in the CA1. These data and model parameters are summarized in Table 2.3.

2.3.6 CA1 and CA2-3-DG show memory-specific cross-frequency coupling changes during retrieval.

For the Retrieval stage, cross-frequency coupling on PAC electrodes was computed during the viewing of quiz images (both targets and lures) corresponding to objects in the MISSED and RECOLLECTED categories. This trial division allowed to compare the signals recorded during retrieval of the same RECOLLECTED and MISSED objects as we assessed in encoding. We hypothesized that TLG coupling will become more pronounced in both CA1 and CA2-3-DG during successful retrieval.

Memory-specific increase in % coupled CA1 and CA2-3-DG electrodes during successful retrieval: We saw that more CA2-3-DG electrodes demonstrated significant TLG coupling during retrieval of successfully recollected vs missed category, as measured by counts of significantly coupled PAC electrodes (53.85% RECOLLECTED vs. 23.08% MISSED),

which supported the first part of our hypothesis. Conversely, while we did observe relatively high percentages of CA1 electrodes participating in TLG coupling during retrieval (74.2% RECOLLECTED and 65% MISSED), we did not observe any significant memory differences,refuting the second part of our hypothesis. However, we also saw a significant memory-specific difference in % CA1 electrodes (87.5% vs. 40.6%) engaged in THG coupling during retrieval of trials in the RECOLLECTED condition. This effect was not expected, and was similar to the effect measured on CA1 electrodes during encoding. These results are summarized in Figure 2.10 (a,c) and Table 2.4.

Memory-specific enhancement in THG coupling strength in CA1 electrodes: We also modeled the effect of memory condition and hippocampal subregion on MI strength during retrieval. We hypothesized that both hippocampal subregions show enhancements in theta low-gamma coupling MI during the RECOLLECTED condition. Two Generalized Estimating Equations (GEE) models with either THG or TLG cross frequency coupling strength were constructed as described in the previous section. Our hypothesis was not supported, as we did not see significant effects in the interaction term of the TLG model. (B= 0.058; Std. Error = 1.321; p =0.965). However, we once again saw a memory-specific significant effect in the interaction term of the THG model, similar to that of encoding (B= -2.252; Std. Error = 1.05; p = 0.032). MI strength on CA1 electrodes during the RECOLLECTED$_{enc}$ group was significantly elevated above threshold $MI_{threshold} = 1.96$, as shown by the estimated marginal means, (Figure 2.10 (b,d), and 95% CIs of the interaction term, suggesting a memory-specific upregulation in THG cross-frequency coupling strength specifically in the CA1 during retrieval as well. These data and model parameters are summarized in Table 2.3.

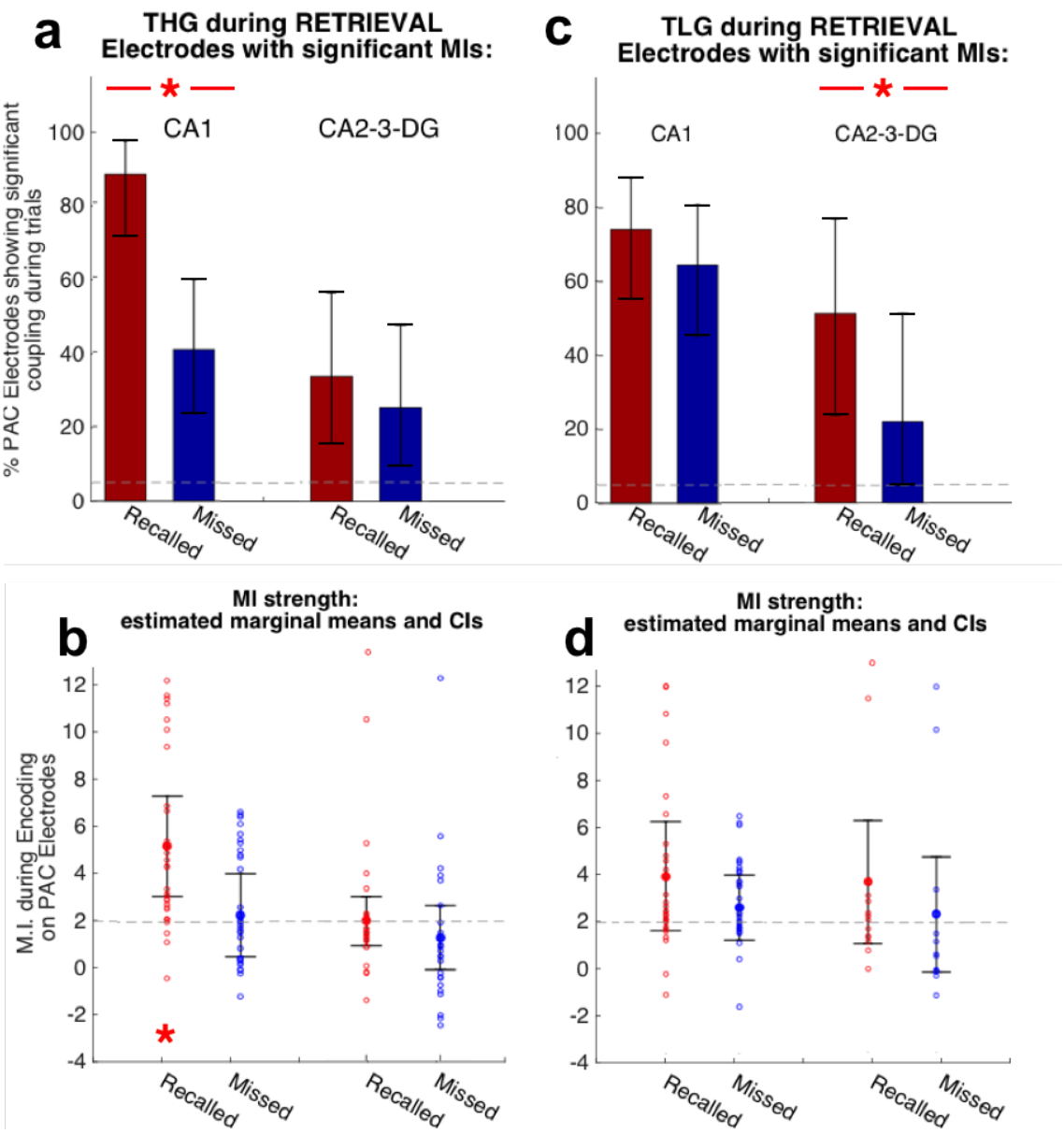

Figure 2.10: Cross-Frequency coupling in CA1 and CA2-3-DG during retrieval of recollected and missed trials

Parameter estimates for GEE models of memory-related theta gamma coupling strength							
Parameter	B	Std. Error	95% Wald CI *(Lower)*	95% Wald CI *(Upper)*	Wald Chi-square	df	Sig.
dependent variable: THG MI_{norm} during encoding							
CA1/CA23DG	2.066	0.89	0.32	3.81	5.392	1	0.02
M/R	-0.18	0.51	-1.18	0.82	0.18	1	0.721
CA1/CA23DG*M/R	-2.45	1.109	-4.62	-0.28	4.89	1	0.027
dependent variable: TLG MI_{norm} during encoding							
CA1/CA23DG	-0.106	1.5813	-3.206	2.993	0.005	1	0.946
M/R	-1.759	0.4427	-2.627	-0.891	15.781	1	0.00
CA1/CA23DG*M/R	-1.115	1.6326	-4.315	2.084	0.467	1	0.494
dependent variable: THG MI_{norm} during retrieval							
CA1/CA23DG	3.470	1.2548	1.010	5.929	7.646	1	.006
M/R	-.700	.4564	-1.594	.195	2.349	1	.125
CA1/CA23DG*M/R	-2.252	1.0494	-4.309	-.195	4.605	1	.032
dependent variable: TLG MI_{norm} during retrieval							
CA1/CA23DG	.217	1.3615	-2.451	2.886	.025	1	.873
M/R	-1.421	.5194	-2.439	-.403	7.479	1	.006
CA1/CA23DG*M/R	.058	1.3206	-2.530	2.647	.002	1	.965

Table 2.3: Parameter estimates for GEE models of memory-related theta gamma coupling during Encoding and Retrieval

Factors: 'Subregion' (CA1/CA2-3-DG),'Memory Success' (M/R —Miss; Recall);Within-subject variable: 'Electrode'

Electrodes displaying memory-related theta-gamma coupling.				
	CA1		CA2-3-DG	
THG–Encoding.				
	R	M	R	M
Percentage of PAC electrodes:	90.625	56.25	55	45
CI_{lower}	74.9773	37.6626	31.5278	23.0578
CI_{upper}	98.0233	73.6362	76.9422	68.4722
TLG–Encoding.				
	R	M	R	M
Percentage of PAC electrodes:	57.1429	19.0476	50	25
CI_{lower}	34.0206	5.4464	21.0945	5.4861
CI_{upper}	78.1803	41.9066	78.9055	57.1858
THG–Retrieval.				
	R	M	R	M
Percentage of PAC electrodes:	87.5	40.625	32	24
CI_{lower}	71.0052	23.6984	14.9495	9.3564
CI_{upper}	96.4869	59.3551	53.5001	45.1288
TLG–Retrieval.				
	R	M	R	M
Percentage of PAC electrodes:	74.1935	64.5161	53.8462	23.0769
CI_{lower}	55.3866	45.3696	25.1345	5.0381
CI_{upper}	88.1436	80.7733	80.7768	53.8132

Table 2.4: Percentages of PAC electrodes demonstrating significant coupling.

All values are percentages of electrodes that are significantly coupled ($MI > 1.96$); Ratios modeled as binomial trials; Confidence Intervals are 95% CIs w/ Clopper Pearson method.

2.4 Discussion

We first asked whether theta gamma coupling is functionally dissociated during encoding and retrieval states, as has been suggested by recent literature [4]. We hypothesized that if theta-high gamma coupling (THG) does in fact facilitate encoding and not retrieval, it will be significantly increased during encoding as compared to retrieval. Our electrode-by-electrode analysis, assessing whether electrodes that are coupled during encoding become quietened during retrieval showed a linear relationship between theta gamma coupling (both TLG and THG), suggesting that the same electrodes that become coupled during encoding are also similarly coupled during retrieval, which did not support our original hypothesis. While we did see a significant subregional difference in theta high-gamma coupling strength, this particular object recognition dataset showed no evidence for functional dissociation between encoding and retrieval. Potentially, such a dissociation would provide evidence of the hippocampal state being primed for either encoding or retrieval by synchronizing subfields to facilitate either entorhinally-driven processes associated with sensory processing and encoding, or, (in the case of TLG) CA3-driven gamma power synchronization associated with retrieval. However, it is possible that encoding and retrieval both depend on strengthened simultaneous communication with EC as well as CA2-3-DG subregion –something that may be expected from a task that presents visually-rich stimuli during both encoding and retrieval stages.

Secondly, we sought to address the growing evidence that theta-gamma coupling affects encoding or retrieval success in a subregion-specific way. We saw that for encoding, wide prevalence of both, THG and TLG coupling in CA1 is crucial for memory success; During trials which are subsequently missed, a drastically fewer percentage of electrodes is in a significantly coupled state for either coupling type. In addition to being more common across electrodes, THG coupling strength also becomes significantly stronger: a significantly higher THG MI index specifically in CA1 is associated with subsequent memory. Stronger MI could result from either more frequent theta-phase locked gamma power bursts, stronger

phase-locked gamma power, or higher gamma specificity.

During retrieval, we hypothesized that TLG coupling will become more pronounced during successful trials in both of our subregions, suggesting CA3-driven hippocampal synchronization utilizing the TLG mechanism. Indeed, significantly more CA2-3-DG electrodes demonstrated significant TLG coupling during retrieval of objects belonging to the successfully recollected vs missed category, as measured by counts of significantly coupled PAC electrodes. However, this finding did not extend to CA1, where TLG coupling showed no differences in memory conditions. This would suggests a role for TLG coupling in CA2-3-DG supporting retrieval success, however this does not support its role as a CA3-CA1 synchronizing mechanism associated with correct retrieval. Finally, we found that CA1 specifically engages in memory-specific THG coupling during retrieval. This perhaps surprising result suggests that CA1 THG is important for memory success in both retrieval as well as encoding, at least in our visually-rich stimulus-driven object recognition task.

Some limitations to these data include potential encoding interference during retrieval. While the encoding part of the task is well-isolated, retrieval may reflect a mixture of encoding and retrieval processes. Hence, the target, lure, and foil stimuli presented during the quiz would strengthen input from EC, and initiate simultaneous retrieval/encoding during the retrieval portion of our task. This could explain the enhanced role of memory-specific THG coupling in CA1 during encoding as well as retrieval. Further, the retrieval data set is susceptible to bias associated with a failure in encoding that may precede any retrieval; it is unclear whether a stimulus was attributed to the 'MISS' set due to an encoding failure or a retrieval failure, and hence, some subset of failed retrieval trials for which we assessed memory-specific THG coupling may have originated because of a failure in encoding, and not retrieval. This particular bias is not easily controlled for with the current task design, and further tasks need to be designed to probe this difference.

Neuropsychiatric scores of the 16 participants						
Subject No.	Verbal IQ *Standard Score*	Digit Span *Percentile*	Verbal Memory *WMS Percentile*	Verbal Memory *CVLT Percentile*	Visual Memory *Percentile*	Executive Function *Percentile*
444	109	25.3	15.9	29.7	4.2	2.3
445	96	18.4	11.5	6.3	2.3	–
447	113	10	66	79	34.5	91
450	98	91	63	49	50	32
452	108	16	50	69	2	46
454	85	47	25	$< 1^b$	< 1	< 1
456	99	8.1	1.1	68	< 1	63
460	114	37	16^a	7	9	16
461	102	16	47	42	53	63
465	118	37	63	84	14	16
466	97	9	16	2	8	2
467	..	..	..	..	..	..
^{a}Verbal Paired Associates Delayed Recall; ^{b}Rey Auditory Verbal Learning Test score						

Table 2.5: Neuropsychiatric Scores

Subject demographics and seizure data.							
Subj. No.	Age	Gender	Handedness	Localizations		Seizure within 2 hrs.	Seizure Onset Zone
				Left	*Right*		
444	24	F	R	-	RAH	no	Extra-temporal
445	37	M	L	LMH	RMH	no	Left orbitofrontal
447	34	F	R	-	RAH	no	Right temporal
450	48	M	R	LMH	RMH	yes	Unknown (subclinical)
452	20	M	R	LAH	RMH	no	Extra-temporal
454	45	M	L	-	RMH	no	Left medial temporal
456	34	F	R	LMH	RMH, RAH	no	Right medial temporal
460	27	F	R	LMH	RMH	no	Right medial temporal
461	20	M	R	-	RMH	yes	Left medial temporal
465	30	F	R	LMH	-	no	Right temporal
466	21	F	R	LMH	RAH	no	Left anterior mesial temporal
467	22	F	L	RAH	LAH	no	Superior to supramarginal gyrus, extended to occip. lobe

Table 2.6: Demographics, hippocampal localizations, and seizure info.

CHAPTER 3

Cross-frequency-coupling in hippocampal iEEG during virtual navigation in trials with and without stimulation of entorhinal white matter

3.1 Introduction

Although the exact role of oscillatory activity in cognition remains unclear, it is thought to represent rhythmic changes in cortical excitability [52] that may result in either minimal or maximal neuronal processing and communication. Intracranial recording of local field potentials (LFPs) in humans have yielded important insights. LFP oscillations specifically within the theta or 3 to 8 Hz frequency in humans [53–55] seem to play an important role in human memory and the strength of their amplitude measured in the human medial temporal lobe (MTL) has been shown to predict the success of learning [53,54,56,57]. Theta resetting, or the phase locking of the theta rhythm with incoming sensory stimuli, has been proposed as one mechanism by which the hippocampus may enhance the encoding of new incoming sensory information and thus enhance memory [58, 59]. Theta resetting has been shown in both rodents and humans during cognitive tasks [16, 59–61]. Electrical oscillations in recordings of the hippocampal local field potential (LFP) have been stipulated to carry information pertaining to encoding and retrieval processes in different frequency bands, which also display cross-frequency associations. Evidence suggests that coupling between the phase of theta (4–8 Hz) and the amplitude of gamma (>30 Hz) oscillations, termed phase-amplitude cross frequency coupling (CFC), may be important for hippocampal-dependent memory. The presence of phase-synchronized low-frequency oscillations and cross frequency coupling have

been shown to be associated with enhanced Long-Term Potentiation (LTP) and spike-timing dependent plasticity (STDP).

Recently, we showed, using a spatial navigation task, a memory benefit for locations learned during deep brain stimulation (DBS) of the entorhinal white matter area compared to locations learned without stimulation. Stimulation of both the fornix and perforant pathways induces resetting of the theta oscillation in the rodent hippocampus [12]. Interestingly, theta activity that predicts recall success is strongly linked to the gamma oscillation (30–100 Hz; [56]). The phase of theta oscillations and their relationship to the amplitude of gamma oscillations in monkeys and humans have been related to memory performance [16, 62]. This has been termed a type of phase-amplitude cross frequency coupling (CFC) and is though to assist with entrainment of internal cognitive processes with external stimuli or events, a process crucial for successful memory formation. Hence, theta-gamma coupling may be a key mechanism by which entorhinal cortex organizes entorhinal communication. In the current study, we aim to test whether hippocampal theta phase and gamma amplitude CFC is enhanced during DBS of the entorhinal area in patients implanted with depth electrodes.

3.2 Methods

3.2.1 Participants

The participants were four neurosurgical patients (all right-handed, 3 female, 20–52 years old, mean age=35.4) with pharmacoresistant epilepsy who were implanted with intracranial depth electrodes for 7–10 days to determine the seizure-onset zone for possible surgical resection. Electrodes were implanted stereotactically using magnetic resonance imaging (MRI) and digital subtraction angiography (DSA) guidance [29, 31]. Electrodes (Adtech, Racine, WI) included platinum contacts for EEG recording and stimulation. Electrode placements were determined solely based on clinical criteria. EEG activity was recorded and analyzed from hippocampal electrodes ipsilateral to entorhinal electrodes. No electrode that was used in this study fell within a determined seizure-onset zone. All subjects volunteered for the study

by providing informed consent according to a protocol approved by the UCLA Medical Institutional Review Board.

3.2.2 Stimulation

Stimulation was current regulated, charge-balanced, with biphasic rectangular pulses set below the after-discharge threshold (based on pretesting; ranged from $1.0mA$ –$2.0mA$). Subjects were blind to stimulation condition and no subject reported noticing any effect of stimulation. Electrode contacts were stimulated through interface with a Grass C-12 stimulator, Telefactor relay box, and Stellate recording system. Stimulation was bipolar (0.059 cm^2 surface area, 1.5 mm apart) with a cycle of 5 sec on and 5 sec off at 50 Hz and 300 μsec pulse length. Current ranged from 0.5 –2 mA with stimulation ranging between 2.5–10.1 $\mu C/cm^2$ per phase, which was well below the safe maximum used for chronic ($30\mu C/cm^2$ per ph) and acute ($57\mu C/cm^2$ per ph) stimulation [63, 64]. The impedance of electrodes measured between 1–4 $k\Omega$. Previous human studies using stimulation parameters of up to 3.0V, $450\mu s$ pulse width and 130Hz, have shown to be safe and well tolerated in patients with epilepsy with depth electrodes in the temporal lobe [65]. A neurologist was present during all sessions to monitor the subject at bedside and view real—time EEG for seizures. No seizures were elicited during stimulation in the current study; similar stimulation levels have been used in clinical studies for seizure control in epilepsy [66].

3.2.3 Behavioral Tasks

Subjects completed a spatial learning task that consisted of navigation through a virtual environment and delivery of passengers to stores (see [14] for further details). The experimental session consisted of alternating blocks of spatial learning and control conditions. Subjects learned to navigate to six stores in a virtual environment; each store was repeated in each of the four blocks (24 total navigation trials). Learning the location of stores under stimulation and no stimulation alternated, and whether learning the first location occurred

under stimulation or not was counterbalanced across subjects. Each store occurred equally often in stimulation and non-stimulation conditions across subjects. During "stimulation" store trials, stimulation was given throughout the entire trial in 5–sec on/off trains; trial duration varied depending on the time needed for the subject to locate the store (Average trial time = 14.76 ± 1.84 sec). (Figure 3.1).

3.2.4 Electrode Localization

Prior to implantation with depth electrodes, subjects were scanned with a Siemens Trio head-only 3 Tesla MRI scanner. For full details on scanning parameters and electrode localization method, see [14]. Stimulation was given using the two most distal contacts of each electrode (Figure 3.2). For entorhinal electrodes the most distal contact was within the entorhinal white matter or alvear bundle/perforant path.

3.2.5 Electrophysiological Analysis

In four subjects with electrodes in the entorhinal cortex and ipsilateral hippocampus, intracranial electroencephalogram (iEEG) data (sampling frequency 200 Hz; frequency band-pass 1–70 Hz) from the hippocampus were analyzed.

Filters for theta-gamma CFC analysis: to assess theta-gamma coupling in *a-priori* predefined frequency bands, iEEG data was filtered for theta (3–8 Hz), alpha (9–14 Hz), beta (15–35Hz), gamma (36–100 Hz), and high gamma (70–80 Hz) utilizing a least squares finite impulse response (FIR) filter (*eegfilt.m* function in the EEGLAB toolbox [47]), and then normalizing each frequency band time series. In order to avoid introducing phase distortion, filtering was performed in a bidirectional manner via the *filtfilt.m* matlab function [47].

Dataset construction: The Stim dataset was constructed by selecting 5-sec. epochs centered on the stimulation onsets for each trial. The Non-stim dataset was constructed by selecting from the nonstimulation trials epochs temporally matched to those in the stimulation trials. Filtering and hilbert-transforms were done on whole records prior to epoch

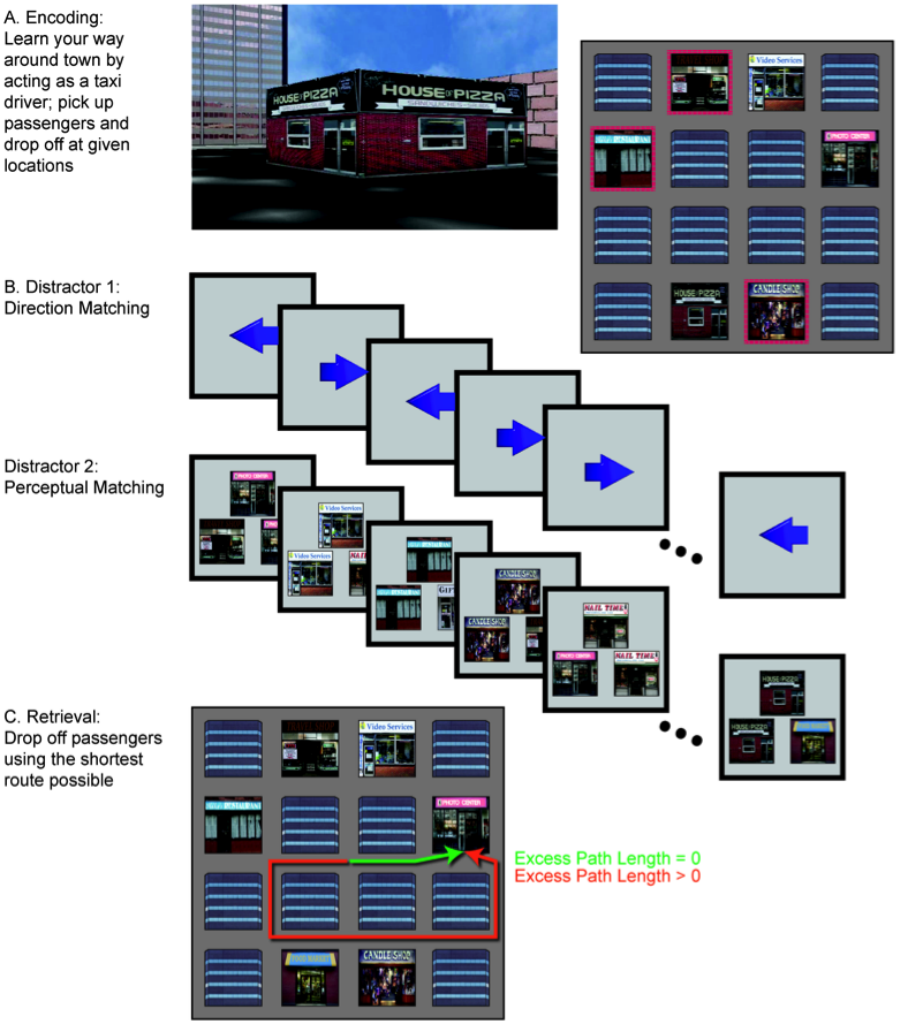

Figure 3.1: Navigation Paradigm and stimulation scheme

a) Top down view of an example virtual city that was used showing stores and buildings. Arrows show behavioral measurement of excess path length. Shorter excess path length (yellow) equals better performance. Red outlined stores show example stores in which stimulation is turned on during navigation. b) Stimuli presented during store—matching task and c) direction—pressing control tasks. d) Experimental paradigm consisted of alternating blocks of navigation and control (Ctl) tasks. Red shows stimulated trials. During block 4 (retention) no stimulation is given on any trial.

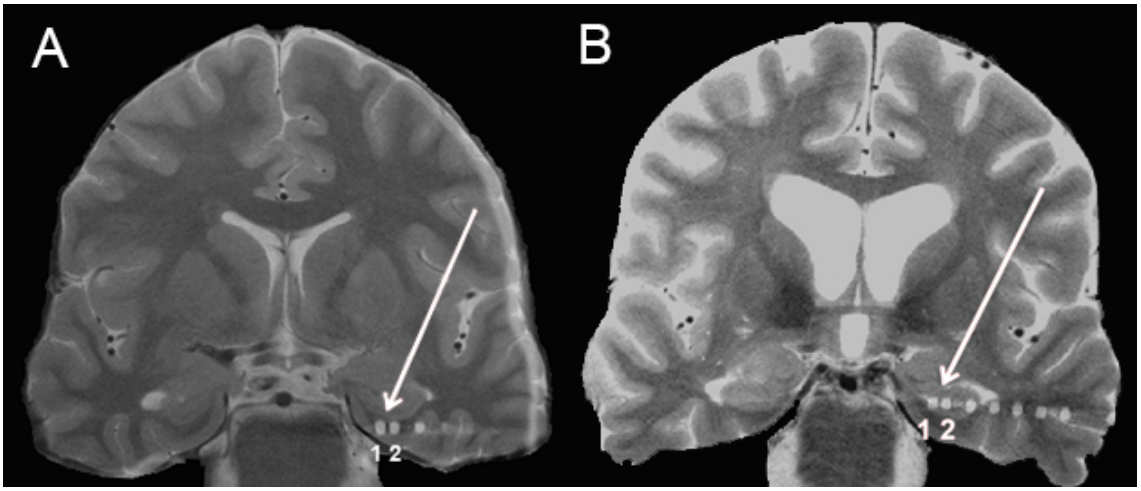

Figure 3.2: An example macro contact localized to Entorhinal white matter a) b)

selection to avoid edge artifacts.

Computing Phase-Amplitude Coupling Cross frequency coupling (CFC) analyses was completed based on previously published methods [48]. To compute hippocampal cross-frequency coupling during stim and non-stim trials, we measured the Modulation Index (MI) between the phase component of a low-frequency (e.g. theta) band Φ_θ, and the amplitude component of a high-frequency (e.g. gamma) band $A_{\gamma high}$ during -2.5—2.5 second epochs surrounding each stimulation onset. For trial-by-trial analysis, all ephocs in a trial were concatenated prior to computing theta-gamma coupling. For example, to determine MI in 1 stimulation trial containing $N = 10$ epochs, an LFP signal pre-filtered at the theta (3–8 Hz) range was converted into a complex-valued signal with the Hilbert transform. All epochs were truncated to time regions $[t_{-2.5} : t_{2.5}]$ surrounding each stimulation onset and re-shaped into a $1 - by - N \cdot [t_{-2.5} - t_{2.5}]$ vector of concatenated epochs for each trial. Then the phase angle time series of this complex-valued signal was measured, resulting in the instantaneous phase of the low-frequency band, Φ_θ. Similarly, the lfp pre-filted at the high-gamma frequency (75—125 Hz) range was used to compute the instantaneous high-frequency amplitude signal $A_{\gamma high}$ consisting of the amplitude (absolute value) of the vector of hilbert-transformed and concatenated epochs. To measure strength of coupling between the theta phase Φ_θ and

gamma amplitude $A_{\gamma high}$, those two signals were combined into an analytic complex-valued signal via Euler's formula, and then the vector mean was computed, with the raw modulation index measured as the resultant vector length:

$$MI_{raw} = \sum_{t=1}^{n} |A_{\gamma high} \cdot e^{i\Phi_\theta}|, \tag{3.1}$$

while the preferred phase is measured as the resultant vector's angle.

Surrogate Analysis: potential autocorrelations in the signal were accounted for by generating 2000 surrogate Modulation Indices, $\{MI_{surr}\}_{1:2000}$, in which the gamma component is shifted with respect to the phase component by a pseudorandomly generated lag value and wrapped. A normalized MI index MI_{norm} is generated by z-scoring against the normal distribution fitted to $\{MI_{surr}\}_{1:2000}$.

Computing normalized-power comodulograms: To create 'stim' and 'non-stim' power coherence comodulograms, first, a set of band-pass filtered signals was created by filtering the lfp signal with an FIR filter centered at all frequencies between 10 and 80Hz, in 2 Hz increments, with ± 2Hz. surrounding each increment (hence each bandpass is 5 hz wide), and then normalizing each bandpass by subtracting the mean and dividing by standard deviation of entire record. Data is filtered with two-way least-squares FIR filtering, utilizing the eegfilt matlab function. Normalization is necessary to compare different frequency bands without the $1/f$ bias. The Hilbert transform is applied to each normalized, band-pass filtered signal in the set to create complex-valued analytic signals, from which the normalized power at each frequency increment was calculated by computing the square of the absolute value of the analytic signal set. Then, data is filtered between 3 and 8 hz to extract theta activity [67], and its phase was computed using the hilbert transform. Theta troughs were localized by finding all time points at which theta reaches a local minima. One-second signal segments centered on these theta troughs were averaged to visualize an averaged, trough-locked theta trace (figure 3.3, bottom panel). 1-sec epochs centered on each theta trough were likewise excised from the normalized power and averaged within each frequency band to compute the theta-trough locked trace of mean instantaneous power across frequencies between 10 Hz

and 80 Hz. The comodulograms for stim and nonstim datasets were visualized on the same scale, with the averaged, trough-centered theta trace on the x-axis, and the theta-trough centered instantaneous averaged power at various frequencies on the y-axis as showing in figure 3.3.

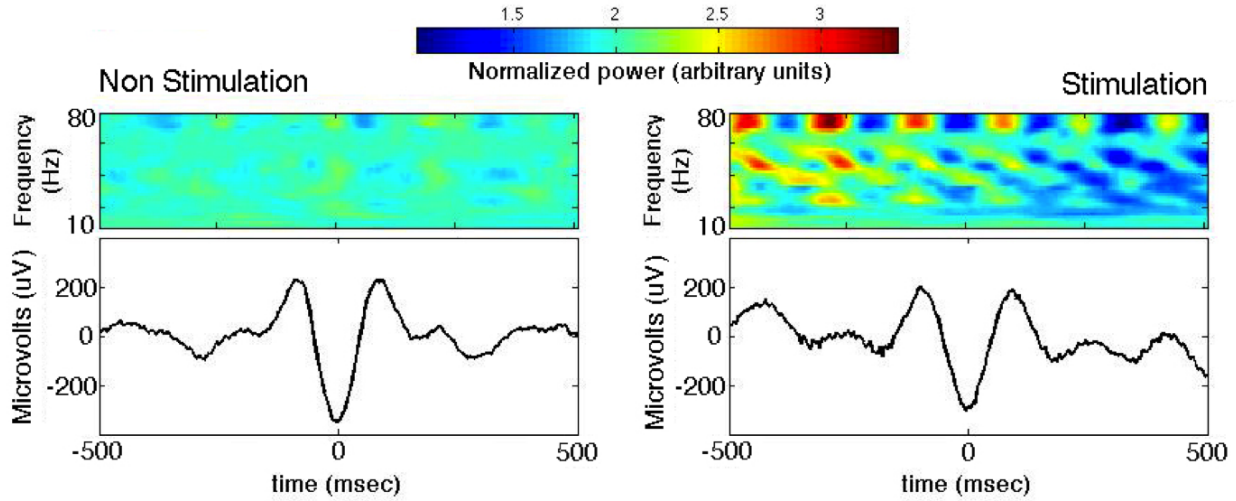

Figure 3.3: Comodulograms for stimulation versus non stimulation conditions

3.3 Results

We calculated the amount of hippocampal cross frequency coupling between the theta (i.e. 3–8 Hz) and gamma (i.e. 30–80 Hz) frequencies. Across all patients and trials, We found a significantly higher CFC during stimulation compared to non-stimulation trials (stim > non-stim, $p = 0.019$). As well as a significant effect of stimulation on gamma amplitude coupling to the phase of a range of low-frequencies ($F(2, 27) = 9.04$, $p = 0.003$; 2-way anova (frequency bands for phase, stim/nonstim trials)), with stimulation optimally enhancing CFC when the phase of coupling was in the low theta range (Figure 3.4). Figure 3.3 shows an example patient's phase-locked modulation of power (comodulogram) from a hippocampal electrode recording during non-stimulation trials of spatial navigation. Our non-stimulation results showing power modulated gamma activity that is time-locked to the theta wave is

similar to that of others [48]. Although we do see significant theta-gamma phase-amplitude coupling during both non-stimulation ($p < 0.05$) and stimulation ($p < 0.05$) trials, there is significantly more theta-gamma CFC during DBS (Figure 3.3; stim > non-stim, $p = 0.019$, wilcoxon rank-sum).

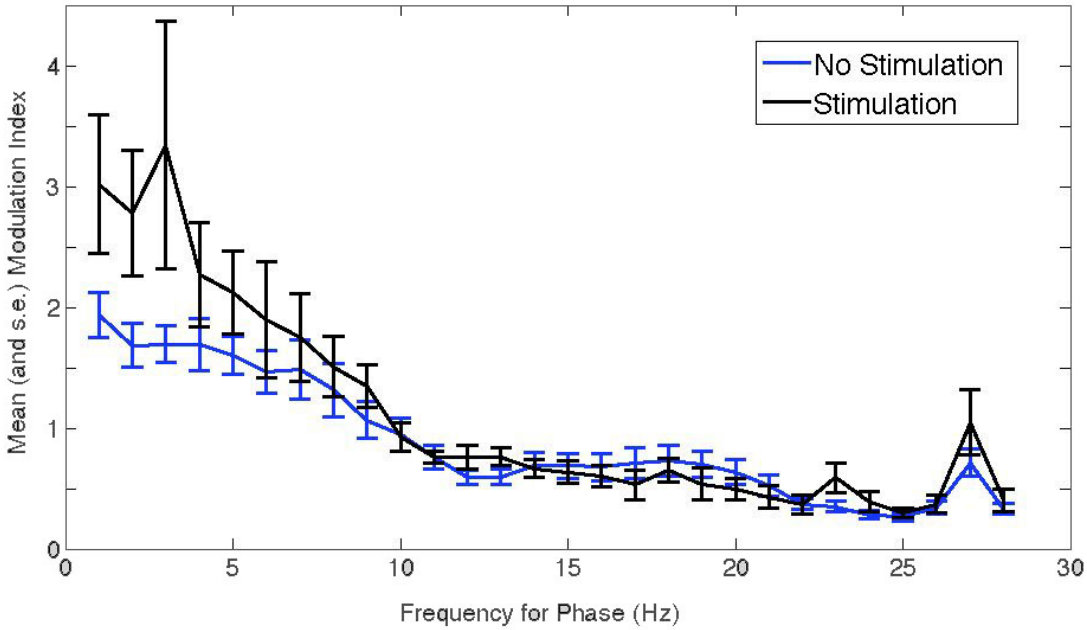

Figure 3.4: Example patient's phase-locked modulation of power from a hippocampal electrode

Shown is the modulation index as a function of frequency for phase. Blue and black curves indicate conditions with no stimulation and with stimulation respectively. Error bars correspond to the standard error of the mean.

Our behavioral results from this study have been previously published (see [14]). In sum, performance on each learning trial was measured by calculating the subjects' latency and excess path length; shorter latency and excess path length corresponded to better performance. On the retention block (block 4), when memory for the store location was tested without stimulation, there was a significant benefit (shorter latency and excess path length) for those locations which had been previously learned during stimulation of the entorhinal region compared to locations which had been learned without stimulation ($N = 18$

trials; $stim > nonstim$, latency: $t(17) = -2.85$, $p < 0.05$, corrected; excess path length: $t(17) = -3.28$, $p < 0.05$, corrected; Cohen's $d = 1.74$). In contrast to the striking effects seen with stimulation of the entorhinal region, direct hippocampal stimulation resulted in no effect on the spatial learning task performance ($N = 18$ trials; $stim > nonstim$, latency: $t(17) = 0.06$, p=n.s., Fig. 3D; excess path length: $t(17) = 0.0161$, p=n.s., Fig. 3B).

3.4 Discussion

Presently, we found a significant increase in theta-gamma CFC during both stimulated and non-stimulated spatial learning with a significantly higher CFC during stimulated compared to non-stimulated trials. These results suggest that DBS of the human entorhinal area that enhances memory results in substantial coupling of theta and gamma oscillations within the hippocampus, suggesting a possible neurophysiological mechanism for stimulation related memory enhancement. These results also support the idea that hippocampal theta-gamma coupling is associated with optimal learning in humans.

Altogether, intracranial studies in humans affording simultaneous LFP and single neuron recordings have begun to link potential mechanisms by which the theta and gamma oscillations together with single neuron activity may support successful episodic memory. Altogether, insight into how external stimulation, single neurons, and oscillatory activity work together to support the successful encoding and recall of individual memories is unknown and an important question partially addressed in given study.

CHAPTER 4

Perturbing the entorhinal-hippocampal system with electrical stimulation: Stimulation of entorhinal white matter enhances declarative memory encoding

The medial temporal lobe (MTL), which includes the hippocampus and adjacent entorhinal, perirhinal, and parahippocampal cortices, plays a critical role in the formation of declarative memories. Deep brain stimulation (DBS) in humans has shown potential promise for improving hippocampal-dependent memory, yet little is known about how stimulating different targets within the MTL affects behavior. Here, we investigated whether DBS of entorhinal white matter vs. adjacent gray matter has differential effects on memory performance in humans. High-resolution magnetic resonance imaging (MRI) and automated image segmentation methods were used to localize stimulating electrodes to entorhinal white matter or adjacent MTL gray matter. Our results indicate that stimulation of entorhinal white matter can enhance declarative memory encoding, while stimulation of neurons in nearby gray matter is ineffective in improving MTL memory function.

4.1 Introduction

The ability to remember new facts and experienced events depends on the hippocampus and associated structures in the medial temporal lobe (MTL), including entorhinal, perirhinal and parahippocampal cortices [1, 2]. In rodents, electrical stimulation of the afferent input to the hippocampus from the entorhinal cortex (i.e., perforant path) has been shown to produce long-term potentiation and acetylcholine release both of which are associated with

improved memory [8–13]. Direct stimulation of the perforant pathway in rodents has also been shown to improve spatial memory and hippocampal neurogenesis [68, 69]. In humans, the perforant pathway is located within the alvear bundle [70] (MTL adjacent white matter area); although human memory studies have not specifically targeted the alvear bundle for stimulation, a few have examined stimulation's effect on the larger MTL region and arrived at contradictory results [14, 71, 72]. In the current study we sought to directly determine whether DBS of this entorhinal white matter vs. the adjacent MTL gray matter, during learning, could account for these differential effects on memory performance. Our results support the hypothesis that stimulation location is key; entorhinal white matter stimulation improved subsequent memory while adjacent gray matter MTL stimulation had no significant effect. This spatially minute distinction could have great clinical relevance for the treatment of memory disorders.

Our data came from a variety of hippocampal-dependent memory tasks (verbal free recall, object recognition, face recognition, face-name association, spatial navigation), and employed both macro- and micro-stimulation, giving us a unique opportunity to examine the robustness and generalizability of the performance effect across task type and stimulation protocol. For all memory tasks in this study, DBS was provided during the learning phase for half of the trials in a within-subjects design. Electrodes were localized using automated segmentation software applied to high-resolution MRI and CT scans. A subsequent memory performance index was computed across all tasks and grouped by location of stimulating electrode to determine the presence of regional differences in stimulation's effects on hippocampal-dependent memory.

4.2 methods

4.2.1 Participants

The study subjects were 22 participants (mean age SD: 34.86 12.28 years, Range: 20–63 years, 8 female, 17 right handed) with pharmacoresistant epilepsy who had been implanted

with intracranial depth electrodes for 7–14 days during which intracranial electroencephalographic (iEEG) activity was monitored to determine epileptogenic zone and guide possible surgical resection. Pre-determined clinical criteria guided placement of the 10–12 electrodes (Adtech), which were implanted stereotactically, with the aid of digital subtraction angiography and magnetic resonance imaging (MRI) [29, 31]. Neuropsychological test scores were determined for subjects including tests of memory and executive function. For each subject, Verbal intelligence quotient (IQ) and digit span (i.e., attention) were calculated using the Wechsler Adult Intelligence Scale [27], verbal memory using the logical memory portion of the Wechsler Memory Scale (WMS; [26]) and long-delay free-recall portion of the California Verbal Learning Test (CVLT; [25]), visual memory using the 30-s delayed version of the Rey-Osterrieth Complex Figure Test [23], and executive function using the Trail Making Test, Part B [24]. All research was carried out at the UCLA Ronald Reagan Medical Center. Before participating in the study, all subjects provided written informed consent on a study protocol approved by the UCLA Institutional Review Board.

4.2.2 Stimulation Parameters

A board-certified neurologist was present for each stimulation session to monitor the clinical iEEG recordings for after-discharges and ensure patient safety. Subjects failed to consciously notice any effects of stimulation, and were unaware of which trials within each behavioral paradigm were stimulated. Stimulation of epileptogenic areas was avoided when possible, no sessions were administered within 2 hours of a seizure and no seizures were elicited as a result of stimulation. Details of each macro- and micro-stimulation protocols are outlined below.

4.2.2.1 Macro-Stimulation

Charge-balanced and current-regulated biphasic rectangular pulses were set below an after-discharge threshold, identified through pretesting with a neurologist, and ranged from 0.4

to 6.0 mA (mean ± SD: 1.508 ± 1.457 mA). A Grass C-12 stimulator and Telefactor relay box (both Astro-Med) or a CereStim R96 Macro-stimulator (BlackRock Microsystems), were used to stimulate the electrode contacts. Bipolar electrodes were spaced 1.5mm apart (surface area, 0.059 cm^2) and electrical stimulation was delivered at 50 Hz and with a 300-μsec pulse width. Stimulation ranged between 2 and 30 μC of charge per square centimeter per phase, which is below the safe maximum level (30 and 57 μC, respectively, for long- and short-term stimulation [63, 64], and electrode impedance ranged from 0.3 to 17.0 $k\Omega$) (mean ± SD: 7.04 ± 5.16 $k\Omega$). Upper limits of stimulation at 3.0 V, with a pulse width of 450 μsec and a frequency of 130 Hz, have been considered safe and well-tolerated by previous patients with epilepsy who have temporal lobe-located depth electrode implants [65], and similar types of stimulation have been used as a method for controlling epileptic seizures [66].

4.2.2.2 Micro-Stimulation

A Blackrock R96 stimulator (BlackRock Microsystems) was used to deliver current regulated micro-stimulation, directed through a 100-µm Platinum-Iridium micro-wire (Figure 4.1, red crosshair). As a safety measure, the impedance was checked prior to each session and determined to be between 10 and 50 kΩ (mean ± SD: 27.10 ± 19.21 $k\Omega$). Each stimulation pulse had current amplitude of 150 μA, a width of 200 μs, and an interpulse interval of 100 μs. A theta-burst stimulation protocol was used (i.e., 4 pulses at 100 Hz, occurring every 200 msec). Each individual pulse delivered a charge of 9.32 $\mu C/cm^2$ with a charge density well below the safety upper limit of 100–150 $\mu C/cm^2$ (for a review, see [73]). For each paradigm, the stimulation preceded each stimulus by 1–3 s and was applied for a 1–3 s duration (i.e., 5 pulse trains/s of 4 pulses/train).

4.2.3 Electrode Localization

A high-resolution post-operative computed tomography (CT) scan (Figure 4.2) was co-registered to a pre-operative whole brain magnetic resonance imaging (MRI) and high-

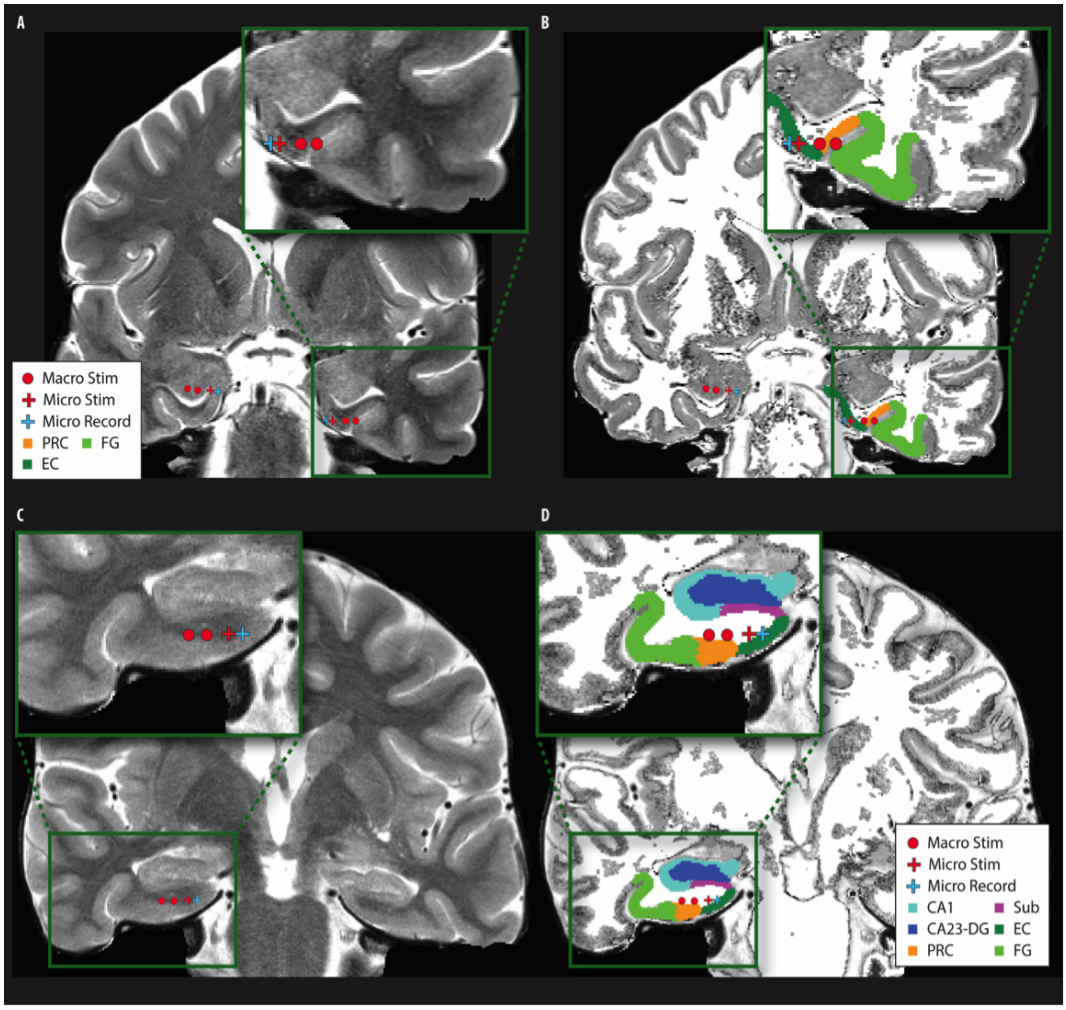

Figure 4.1: Examples of co-registration and automated segmentation methods for electrode localization

(Micro Stim = 100μm micro-electrode, Micro Record = 40μm micro-electrode, Sub = subiculum, EC = entorhinal cortex, PRC = perirhinal cortex, FG = fusiform gyrus) Example subject electrode locations (macro-electrodes and micro-electrodes) overlaid onto the original high-resolution (A, C) and segmented MRI (B, D). Macro-stimulation was delivered to the two macro-electrode contacts and micro-stimulation to the 100-µm micro-electrode. Example automatic segmentations of MTL subregions are shown with delineated hippocampal (CA1, CA3-DG, subiculum) and cortical areas (entorhinal, perirhinal, and fusiform). Bottom is an example bipolar macro-electrode placement within the entorhinal white matter region; top is an example micro- and macro-electrode placement within nearby gray matter regions.

resolution MRI (Figure 4.1) using BrainLab stereotactic and localization software (www.brainlab.com; [35,36]) and FSL FLIRT (FMRIB's Linear Registration Tool [37,38]). Medial temporal lobe regions (entorhinal, perirhinal, parahippocampal, and hippocampal subfields CA23DG [CA2, CA3, dentate gyrus], CA1, and subiculum) were delineated using the Automatic Segmentation of Hippocampal Subfields (ASHS [39, 40]) software using boundaries determined from MRI visible landmarks that correlate with underlying cellular histology [41,42]. White matter and cerebral spinal fluid areas were outlined using FSL FAST software [43]. Together, similar methods have been previously used to localize micro-electrodes and investigate structural and functional dissociations within human medial temporal lobe subregions [44–46]. Each electrode contained macro-electrodes, spaced at 1.5 mm intervals along the shaft (most distal 2 contacts were used for macro-stimulation), a single $100 - \mu m$ micro-electrode (used for micro-stimulation) at the distal tip 3 mm from the most distal macro-contact, and a bundle of seven 40-µm micro-electrodes (not used for stimulation) 5 mm from the most distal macro-contact. Macro- and micro-electrode contacts were identified and outlined on the post-operative CT scan. To determine whether each micro- or macro-electrode fell within white or gray matter, the high-resolution MRI, with ASHS and FAST segmentation results, was overlaid with the co-registered electrode. At minimum, if the more distal of the two stimulating macro-electrodes fell within a white matter region, it was classified as "white." The co-registered CT electrode locations and high-resolution MRIs of example subjects are shown in Figure 4.1 and Figure 4.2. For the placement of each stimulated electrode, see Table 4.7, which includes both the localization result for each electrode as well as the corresponding clinical label. It is important to include both pieces of information, due to the fact that clinically targeted electrode placements are subject to variability.

4.2.4 Behavioral Paradigms

Participants completed at least one of the following five behavioral tasks that were designed to probe hippocampal dependent memory. All tasks shared the same basic structure where each began with a learning (encoding) period, followed by a 30-second distraction task, and

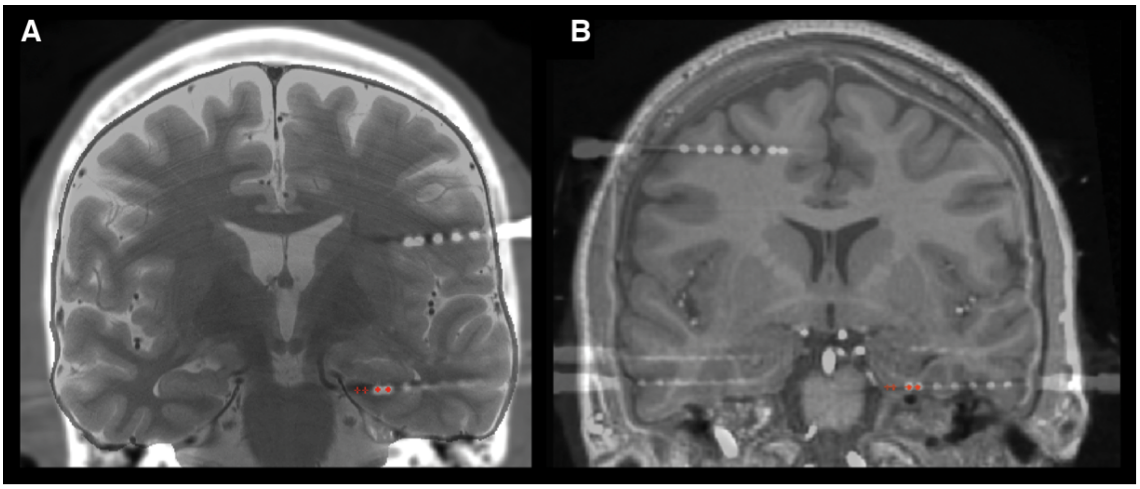

Figure 4.2: Co-registered MRI and CT scans

Shown are example co-registrations of high-resolution MRIs overlaid onto corresponding high-resolution CTs. Two example subjects are shown. (A) A subject with electrodes in entorhinal white matter. (B) A subject with electrodes in adjacent MTL gray matter. Macro electrodes are shown as red dots, while micro-electrode locations are presented as red cross-hairs.

then a test (retrieval) period. For each paradigm, the number of learned stimuli was pre-determined based on neuropsychological testing and/or pre-testing sessions so as to prevent a ceiling or floor effect. Electrical stimulation was provided prior to the onset of stimulus presentation during half of all encoding trials in a randomized fashion within each patient using a within-subject design. The distractor task was identical for each paradigm (except the Spatial Memory task), which included a 30-second odd/even task in which numbers were presented quickly, at 0.6-.75 second intervals, and participants were instructed to classify them as odd or even by using 1 of 2 key presses. For the spatial memory task, two distractor tasks were used. In the first distractor task, subjects were shown left or right arrows on the computer screen and instructed to press 1 of 2 corresponding buttons on a joystick. The second distractor task involved perceptual matching —the subject was presented with a target store image and asked to select the matching store by pressing a corresponding button. For each experimental session, a board-certified neurologist was present to look for

after-discharges in iEEG activity and monitor the patient at bedside. The specifics of each behavioral paradigm are detailed below and example stimuli from each task are shown in figures below.

4.2.4.1 Verbal Free Recall Task

Subjects were instructed to learn a list of 10–20 words that were randomly presented in audio and visual format on a computer screen. Each word was presented for 2 s with inter-trial fixation periods of 4 s. Words were drawn from clusters six and seven of the Toglia and Battig (1978) [74] word norms and were all 4–8 letter nouns that were rated as highly familiar (range 5.5–7 on a 1–7 scale), moderate to high on concreteness and imagery (range 4.5–6 on a 1–7 scale), and moderate in pleasantness (range 2.5–5.5 on a 1–7 scale). Stimulation was applied for a duration of 1–3 s, beginning 1–3 s prior to a randomly selected half of stimuli and terminating before stimulus onset. Following each set of learned words, subjects completed the odd/even distractor task and were then prompted to verbally recall as many words as they could remember during a 30–54 s period (exact duration of retrieval period was dependent on the number of words presented during encoding: number of words multiplied by 3 s). Memory performance for a particular condition (e.g. stimulated or not stimulated) was calculated as the proportion of presented words from that condition that were recalled (Figure 4.3).

4.2.4.2 Object Recognition task

This task was identical to the task described in chapters 2 and 3 of this thesis.

During the encoding stage, subjects were presented with a series of 30–46 images depicting everyday objects that were downloaded from Google Image Search and the Hemera Object Database [75]. A performance measure (discrimination index [DI], described below) was used to rate each image, based on the mean behavioral results of nineteen undergraduate students from the UCLA Psychology Department Subject Pool; the top and bottom 10% of

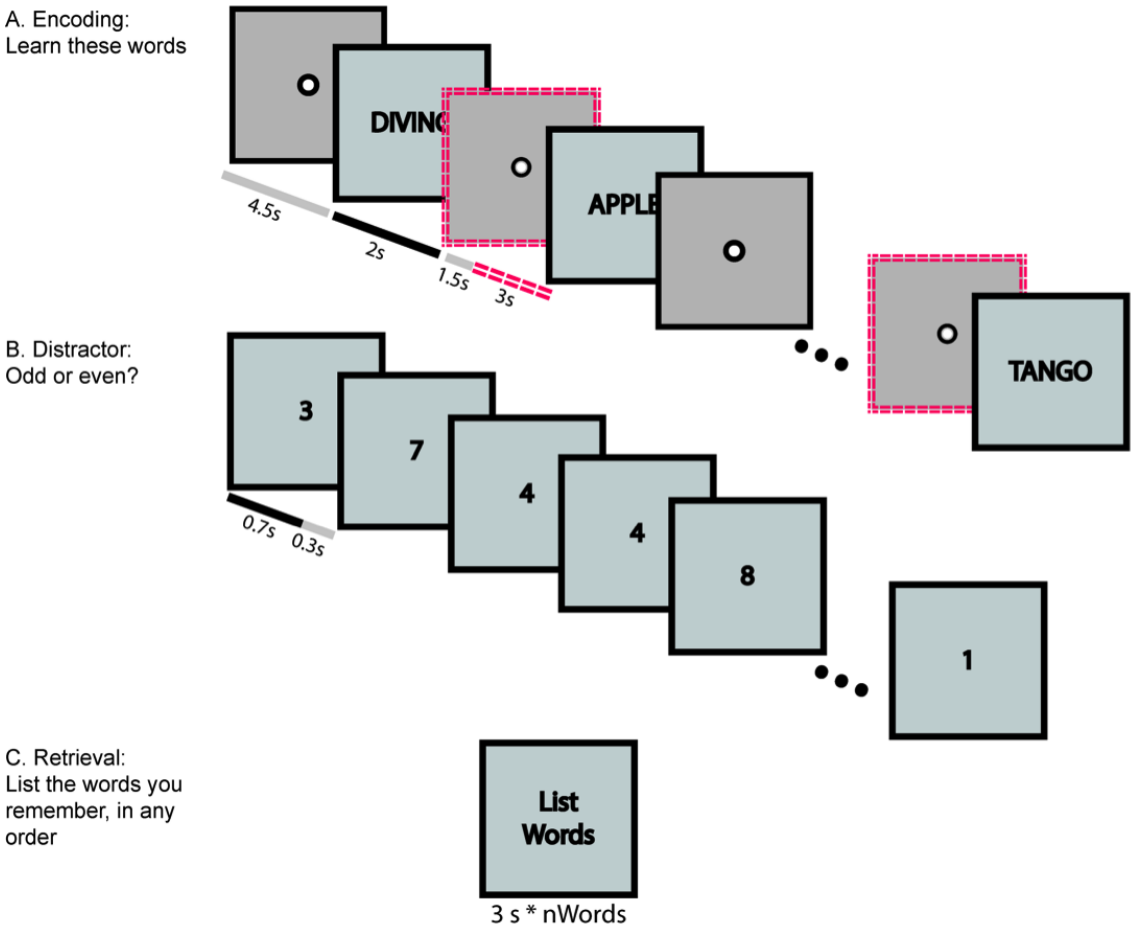

Figure 4.3: Verbal free recall task

During the encoding stage, subjects were shown a list of words, one at a time, and interleaved with fixation periods. Half of the words were selected at random to receive stimulation, denoted above by double, red, dotted lines. In the example above, "apple" and "tango" were considered stimulated words because stimulation was applied during the fixation period prior to word onset. (B) After encoding, subjects were asked to do a 30 s distractor task. Randomly selected single digit numbers were rapidly presented, and subjects had to press the left or right arrow to indicate whether each number was odd or even. (C) Subjects were given time (number of words multiplied by 3 s) to list any words they could remember from the encoding stage.

rated words were removed from the stimulus database to achieve suitable task difficulty level. To promote task engagement, subjects were instructed to determine whether each presented object was "bigger or smaller than a shoebox" and to answer by key press. Images were shown for 4 s and interleaved with jittered fixation periods of 4–4.6 s. Macro-stimulation was applied for the contiguous 3 s prior to a randomly selected half of stimuli, and micro-stimulation was applied for a duration of 1–3 s, beginning 1–3 s prior to a randomly selected half of stimuli and terminating before stimulus onset. Subjects then completed the odd/even distractor task. For each image shown during encoding, three images were shown, in random order, during the retrieval stage. These included the original image ("Target"), a very similar image ("Lure"), and a dissimilar image from the same object category ("Foil"). Subjects were given up to 10 s to rate each image (average response time = 1.95 s; SD = .44 s) on a six-point confidence scale, where "1," "2," and "3" indicated that the image was "new" (not seen during encoding) and "4," "5," and "6" indicated that the image was "old" (already viewed). Ratings of "1" and "6" indicated high confidence ("definitely"), "2" and "5" indicated medium confidence ("probably"), and "3" and "4" indicated low confidence ("maybe"). Performance on this task was measured by the DI [76], which was calculated for each condition.

4.2.4.3 Face Recognition task

Subjects were instructed to learn a series of images of non-famous people presented serially on a computer screen for 4 seconds each, preceded by a jittered interval of 4.5 seconds (± .5 sec). This was followed by the odd/even distractor task. For the retrieval phase, a randomized shuffled image set of previously seen photographs (target images) and similar-looking photographs (lure images) were presented, during which subjects rated their familiarity on a continuous scale from -100 (unfamiliar) to 100 (familiar). The DI was calculated for both stimulated and non-stimulated conditions, identical to that computed in the object recognition task (Figure 4.5).

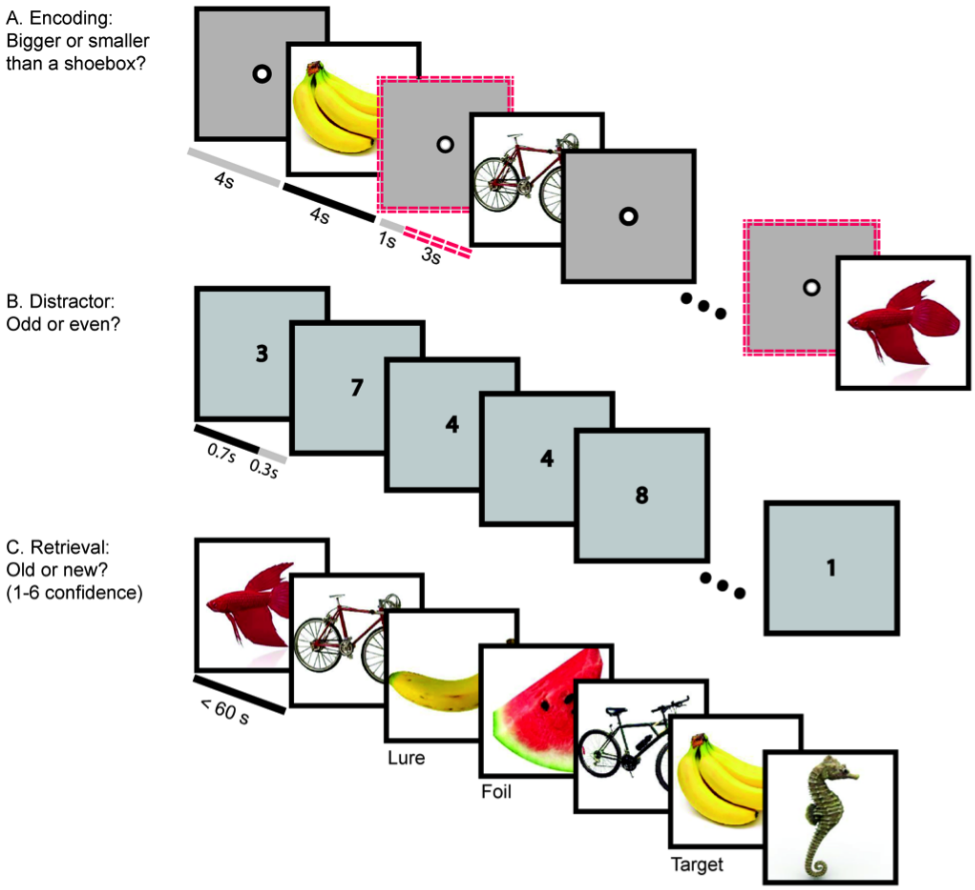

Figure 4.4: Object recognition task

(A) During the encoding stage, subjects were shown a series of objects, interleaved with fixation periods. To promote task-engagement, subjects were asked to indicate whether each item was "bigger or smaller than a shoebox". Half of the images were selected at random to receive stimulation, denoted above by double, red, dotted lines. In the example above, the bicycle and the fish were considered stimulated images because stimulation was applied during the fixation period prior to image onset. (B) After encoding, subjects were asked to do a 30 second distractor task. (C) For each image shown during the encoding stage, three images were shown, in random order, during the retrieval stage. These included the original image ("Target"), a very similar image ("Lure"), and a dissimilar image from the same object category ("Foil"). Subjects were given up to 60 s to rate the image on a six-point confidence scale, where "1" indicated the image was "new" (not seen during encoding) and "6" indicated the image was "old" (i.e., already viewed).

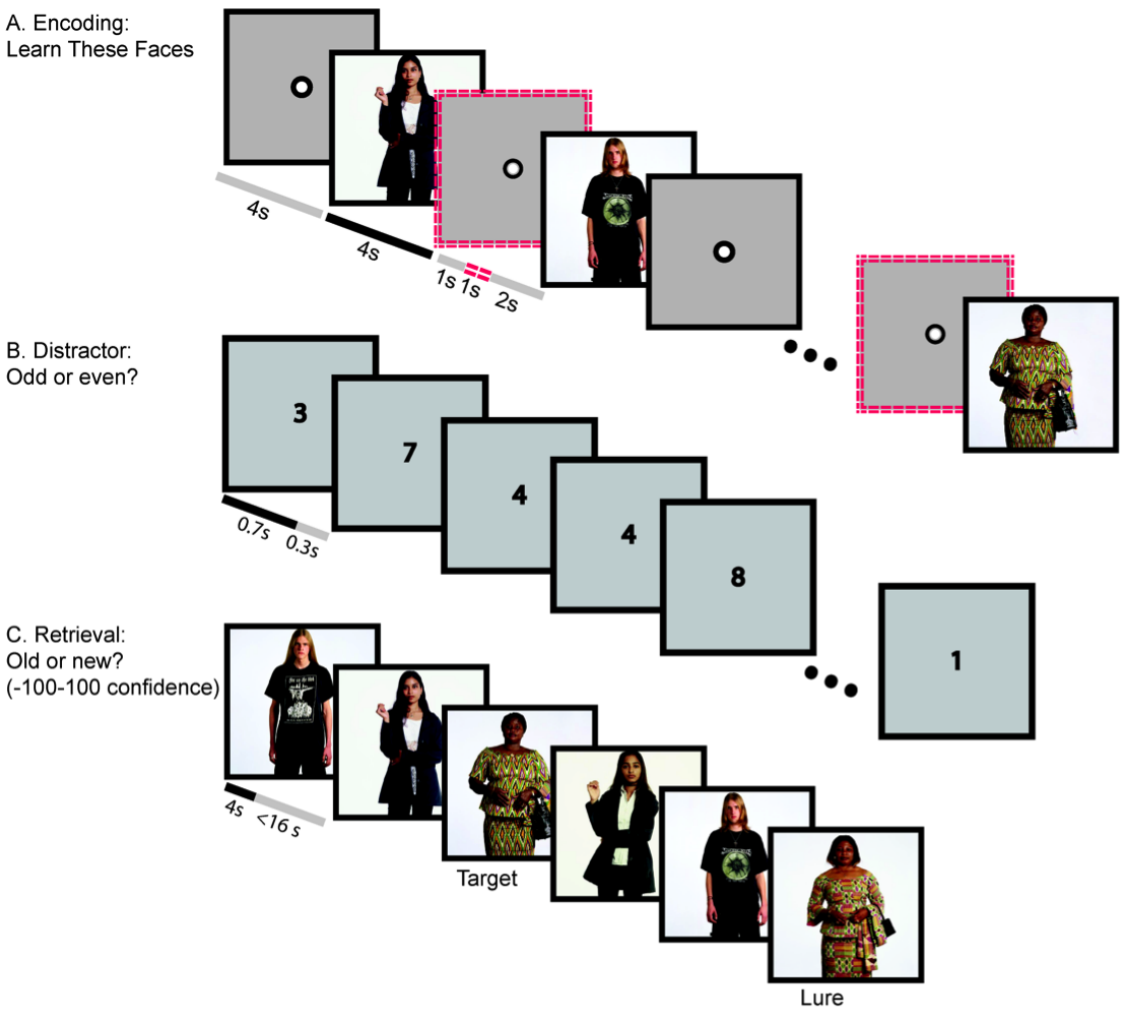

Figure 4.5: Face recognition task

A) During the encoding stage, subjects were shown a series of images of novel people, one at a time, and interleaved with fixation periods. Half of the images were selected at random to receive stimulation, denoted above by double, red, dotted lines. (B) After encoding, subjects were asked to do a 30 s distractor task. (C) For the retrieval stage, a shuffled image set of previously seen photographs ("Targets") and similar-looking photographs ("Lures") were presented for 4 seconds each, and subjects were given up to 16 seconds to rate whether the images were "new" or "old" and assessed their confidence.

4.2.4.4 Face-Name Associative Memory task.

Subjects were presented with a series of either 16 or 32 (depending on individual subjects' pre-testing and neuropsychological memory scores) novel face-name pairs and instructed to learn each pairing. Each face-name pair was shown for 4 s, interleaved with fixation periods of the same duration. Stimulation was applied for either 1 or 3 s, beginning 3 s prior to a randomly selected half of stimuli. Following the odd/even distractor task, each image shown during the encoding stage was presented again, in random order. Subjects were given 4 s to recall the name associated with each image. For patients with especially poor memory, the first letter of the name was presented as a cue; across the 10 stimulated brain regions for this task, 5 sessions were cued for 2 patients across 4 brain regions during recall. After the retrieval phase, the experiment began again with the encoding phase, using the same set of images (with the same subset of images receiving stimulation) to give subjects another opportunity to learn the associations. In total, subjects saw each set of images six times. Memory performance was calculated as the percentage of correctly identified names, averaged across all six blocks, for stimulated and non-stimulated trials (Figure 4.6).

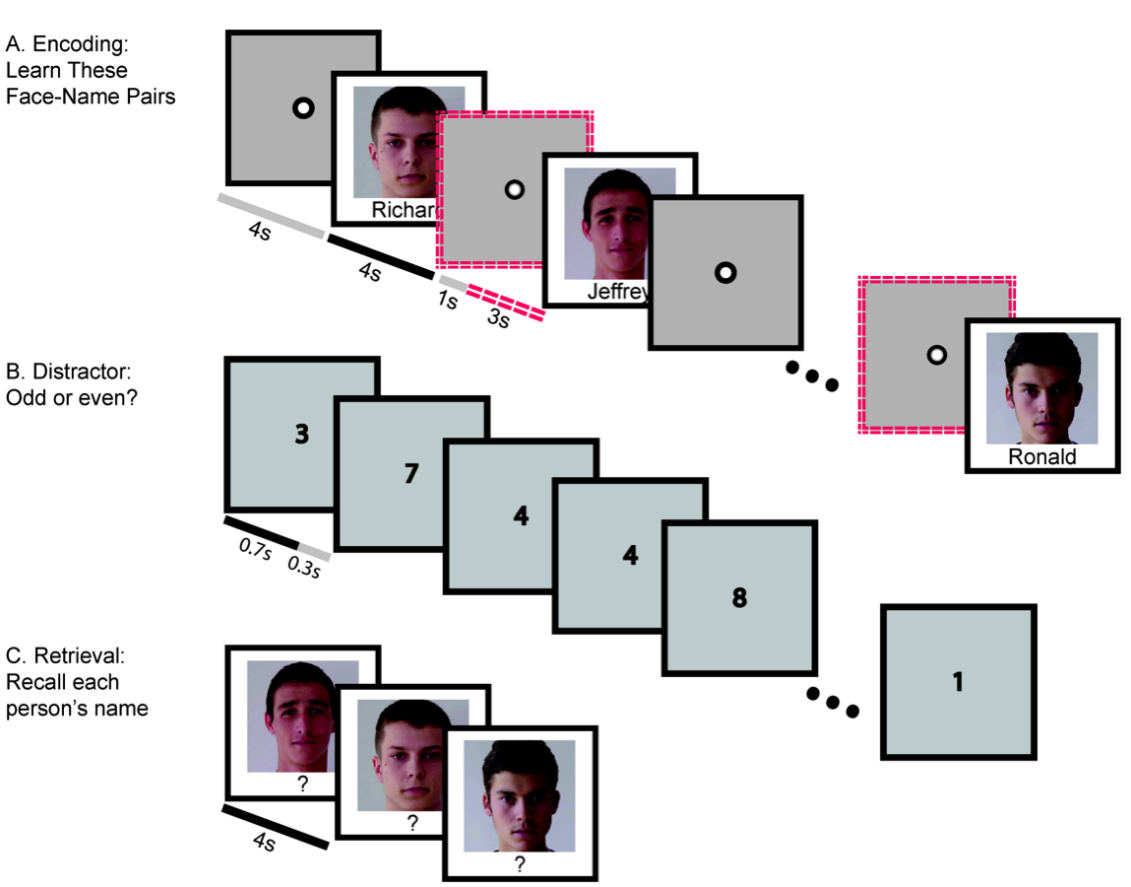

Figure 4.6: Face-name associative memory task

(A) During the encoding stage, subjects were shown a series of images of novel face-name pairs, one at a time, and interleaved with fixation periods. Half of the images were selected at random to receive stimulation, denoted above by double, dotted lines. (B) After encoding, subjects were asked to do a 30 s distractor task. (C) Each image shown during the encoding stage was presented again, in random order. Subjects were given 4 s to recall the name associated to each image. In some cases, subjects were cued with the first letter of the name.

4.2.4.5 Spatial Memory task

During the encoding stage, subjects navigated around a virtual town, acting as taxi drivers. After locating a passenger, the subject was instructed to drop the passenger off at a particular store in town. Half of the stores were randomly selected for stimulation, such that stimulation

was applied in a 5 s on/off manner while the subject was navigating to these stores. After encoding, subjects were asked to complete the two distractor tasks, described above. The navigation/distractor task block was repeated three times, with stimulation applied to the same subset of stores. During the fourth navigation block, no stimulation was applied, allowing for measurement of spatial memory retrieval. Spatial memory performance was measured as "excess path length", calculated by subtracting the length of the ideal path to target store location from the length of the actual path to the store for each trial. Shorter excess path length indicated better performance by the subject. For further details on this task, see previous study ([14], Figure 4.7).

4.2.5 Statistical analysis

In order to compare the effects of white and gray matter stimulation on behavior across experimental paradigms, each task-specific average memory performance score for stimulated and non-stimulated conditions was first converted to an average percent difference score for each subject testing session. To compute the average percent difference score, non-stimulation scores were subtracted from stimulation scores (except for in spatial memory tasks where stimulation scores were subtracted from non-stimulation scores since lower excess path length indicates better memory performance), then divided by the averaged value between non-stimulation and stimulation and converted to a percentage. These percentage difference score calculations allow for positive values to indicate better memory performance with stimulation across all tasks. Percent difference scores were averaged across experimental paradigms for a given stimulation electrode location for each individual subject, resulting in a single value for each electrode location. In other words, this yielded a final, cross-paradigm difference score per subject, per stimulation electrode location, denoted as the performance index.

We used non-parametric Wilcoxon rank-sum test to compare distributions of linear variables (performance indices) and Wilcoxon sign-rank test to assess whether the medians of the distributions were significantly different from zero. To determine the contribution of

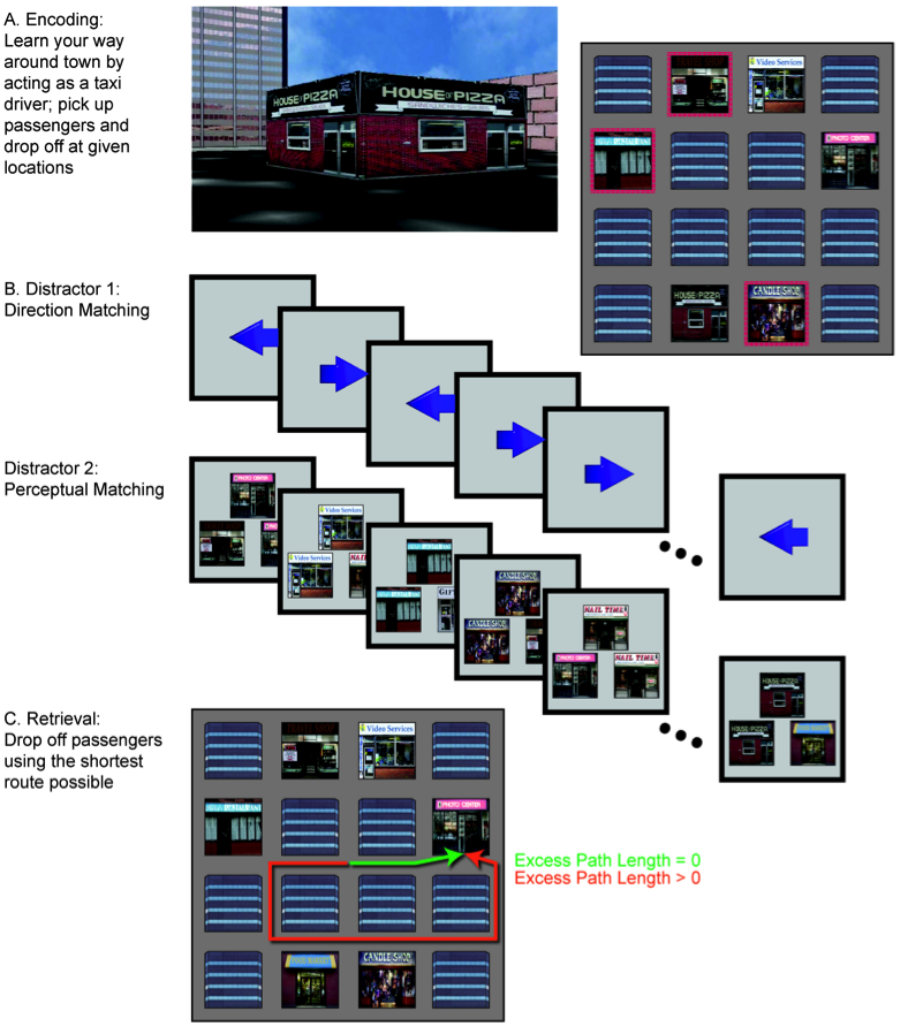

Figure 4.7: Spatial memory task

(A) During the encoding stage, subjects navigated around a virtual town, acting as taxi-drivers. After locating a passenger, the subject was instructed to drop the passenger off at a particular store in town. Left: a passenger-eye view of one store; right: a top-down map of the town. Half of the stores were randomly selected for stimulation, indicated by a red double dotted line. (B) After encoding, subjects were asked to do two distractor tasks. Top: subjects pressed arrow keys matching directions presented on screen. Bottom: subjects selected which of two store images matched a template image presented on screen. The navigation/distractor block was repeated three times. During the fourth navigation block, no stimulation was applied, allowing measurement of spatial memory retrieval in the absence of stimulation. (C) Performance was measured as "excess path length". See Methods.

multiple variables to the performance index, we also performed an ordinary least squares regression in which performance index was modeled as a function of different categorical variables. These predictors included stimulation site (white/gray matter), stimulation type (micro/macro), hemispheric location (left/right), and whether or not anti-epileptic drugs were being administered at the time of stimulation.

4.3 Results

4.3.1 White matter stimulation, but not grey-matter stimulation enhanced memory

Twenty-four subjects with intracranial depth electrodes implanted for clinical epilepsy evaluation participated in the study. Demographics and neuropsychological test scores are shown in Tables 4.5,4.6, and 4.1. Amongst the 24 subjects in the study, a total of 41 electrode sites were used to deliver electrical stimulation. Based on the results of an automated localization procedure, twenty electrode locations (five in left hemisphere) were determined to be in white matter and 21 in gray matter (11 in left hemisphere) (Figure 4.1 and Tables 4.3,4.4).

Performance index scores were calculated, per electrode, by taking the percentage difference of performance scores in stimulated vs. non-stimulated trials and averaging these across experimental tasks. We found that change in memory performance with white matter stimulation was significantly better than with gray matter stimulation (Figure 4.8; p = .006, Z = 2.73, Two-sided non-parametric Wilcoxon Rank-sum test). Specifically, white matter stimulation significantly improved memory (Figure 4.8; median, $[25^{th}, 75^{th}$ percentile] = 21.53, [2.12, 50.72]; p = .009, Wilcoxon Signed-rank test, $N_{white} = 20$) while gray matter stimulation showed no statistically significant memory effect (Figure 4.8; median, $[25^{th}, 75^{th}$ percentile] = -4.71, [-19.78, 6.68]; p = .24, Wilcoxon Signed-rank test, $N_{gray} = 21$). Performance indices from individual paradigms resulted in qualitatively similar results (Figure 4.9).

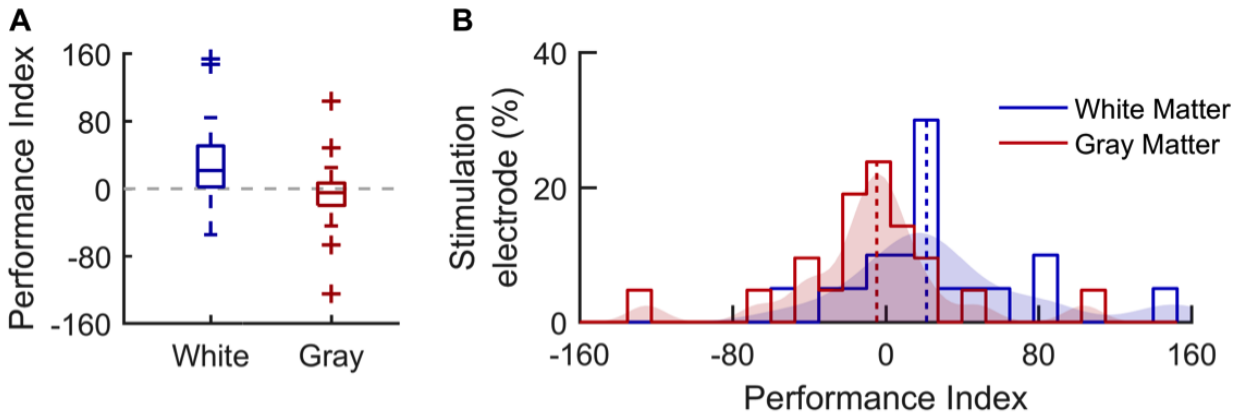

Figure 4.8: White and gray matter distributions by performance index

(A) Performance index is a percentage difference score calculated for stimulated vs. non-stimulated trials, averaged across memory tasks for a given electrode region. Positive performance index indicates memory for stimulated trials was better than non-stimulated trials. Entorhinal white matter stimulation (blue) during learning resulted in improved performance (significantly positive); nearby MTL gray matter stimulation (red) showed no significant effect. (B) Distribution of memory performance index scores for each individual electrode region separated by location: white (blue) and gray (red) matter. Vertical dashed lines indicate median values.

In order to test the main hypothesis while accounting for other variables that could play a role in performance index, we used ordinary least squares linear regression to predict percentage difference scores from electrode location (white/gray), as well as stimulation type (micro/macro), hemispheric location (left/right), and whether or not anti-epileptic drugs (AEDs) were being administered at the time of stimulation (see Table 4.2). Corroborating the previous nonparametric tests, electrode placement in white or gray matter significantly predicted percent difference scores, while hemispheric location, stimulation type, and the presence of AEDs showed an insignificant correlation to this performance index (Table 4.2).

Paradigm	Hemisphere(s) Stimulated	Mean Age	Handedness
Verbal Free Recall	R: 3 / L: 2 / Both: 2	32.57 (SD=17.17)	5 right-handed, 1 ambidextrous
Object Recognition	R: 1 / L: 2 / Both: 1	33 (SD=12.53)	2 right-handed
Face Recognition	R: 7 / L: 4 / Both: 1	36 (SD=12.21)	9 right-handed, 1 ambidextrous
Face-Name	R: 2 / L: 0 / Both: 3	36 (SD=13.44)	4 right-handed
Spatial Memory	R: 4 / L: 1 / Both: 1	32.67 (SD=9.50)	5 right-handed, 1 ambidextrous
TOTAL	**R: 17 / L: 9 / Both: 8**	**34.75 (SD=12.72)**	**18 right-handed, 3 ambidextrous**

Table 4.1: Stimualted hemisphere for different subjects

Shown is the number of participants in each task who received stimulation on the right only (R), left only (L), or in each hemisphere (in different experimental sessions) (Both). Note some brain regions were stimulated for more than one behavioral task, and therefore the total number of hemisphere(s) stimulated does not match the sum of hemisphere(s) stimulated in each individual task.

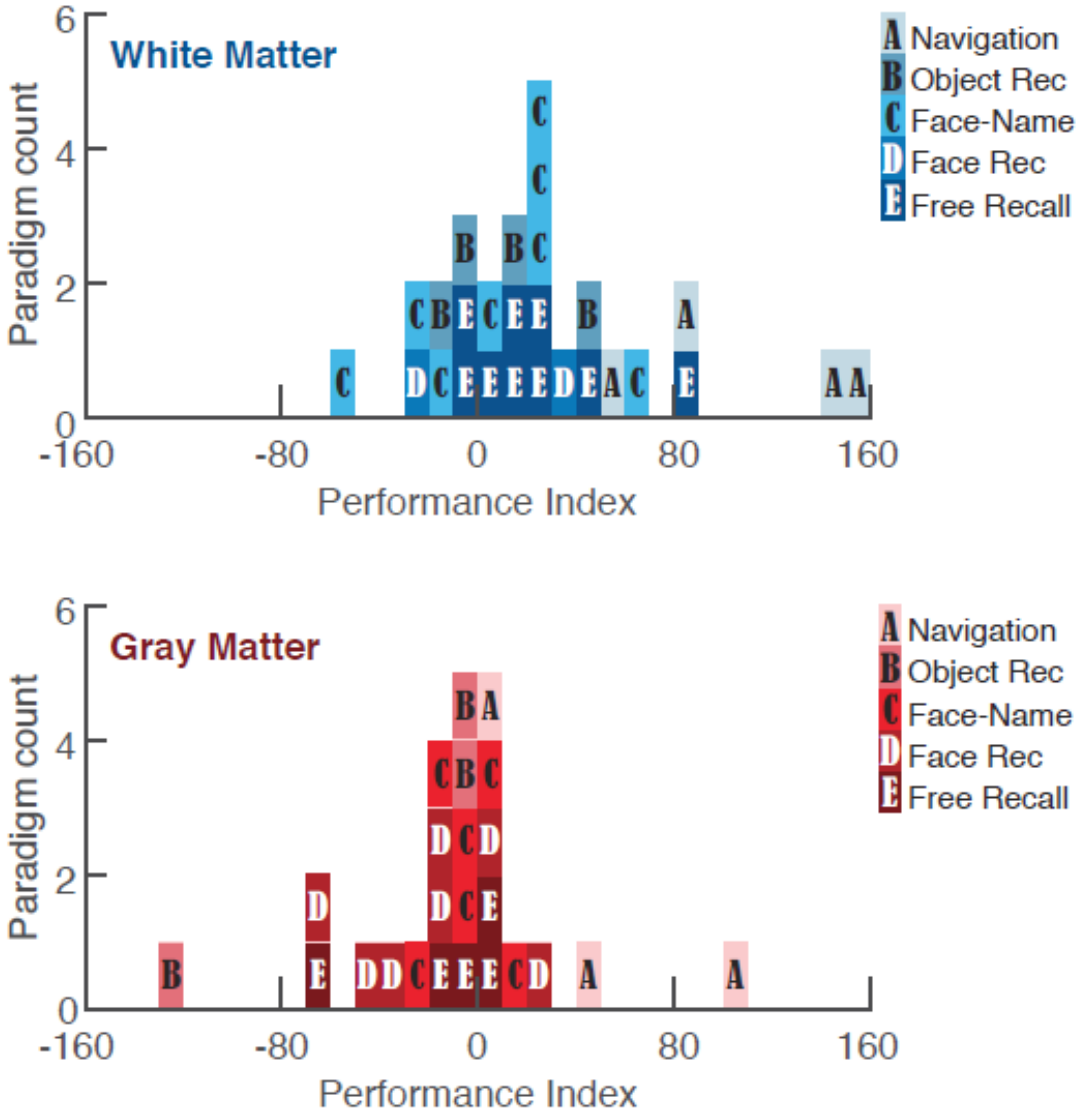

Figure 4.9: Distributions of performance index, divided by task

Shown is the distribution of performance index divided by behavioral task for electrodes in medial temporal (A) white and (B) gray matter. Performance index is a percentage difference score calculated for stimulated compared to non-stimulated trials for a given electrode region, and, for this figure only, not averaged across memory tasks. Positive performance index indicates memory for stimulated trials was better than non-stimulated trials. Negative performance index indicates memory for non-stimulated trials was better than stimulated trials.

	White/Gray			Left/Right			Macro/Micro			AEDs/no		
	β	t	p	β	t	p	β	t	p	β	t	p
All Electrodes[a]	-.477	-3.137	.003 d	.022	.145	.886 d	.371	2.335	.025d	.031	.199	.843[d]
All Electrodes[b]	-.457	-3.013	.005 d	.023	.150	.881 d	.393	2.475	.018d	.049	.319	.752[d]
Non-epileptogenic electrodes[c]	-.572	-3.305	.003 d	.025	.144	.887 d	.412	2.200	.037d	.004	.023	.982[d]

Table 4.2: Ordinary least square regression

The results of using ordinary least squares linear regression to predict percentage difference scores from electrode location (white/gray), hemispheric location (left/right), stimulation type (micro/macro), and anti-epileptic drugs (AEDs); a Using 'discrimination index' as the performance measure for object and face recognition tasks, R2 = .293, F(4, 35) = 3.619, p = .014; b Using 'fraction recalled' ("n Recollected" ‖ "n Trials") as the performance measure for object and face recognition tasks, R2 = .295, F(4, 35) = 3.658, p = .014; c Using 'discrimination index' as the performance measure, excluding electrodes that were determined to be in epileptic regions, R2 = .282, F(4, 26) = 3.941, p = .012.; d A Bonferroni correction was applied to our alpha level as a result of running multiple linear regression tests on the same data, so coefficients were considered significant at a level of $\alpha = 0.05$, when p < .0167 (that is α/n, where n is the number of tests performed).

4.3.2 Hemisphere of stimulation has no effect on memory

To further test the results within each control condition, we examined whether differences in stimulation hemisphere (left vs. right) or stimulation type (micro vs. macro) could account for the observation that stimulation divergently improved or impaired memory.

There was no statistically significant difference between memory performance scores with left or right MTL stimulation, (Figure 4.10; p = .09, Z = -1.7, Two-sided non-parametric Wilcoxon Rank-sum test) and neither left nor right MTL stimulation had an overall effect on memory performance when calculated across both white and gray matter stimulation; however right MTL stimulation had a trend toward performance increase (Left: median, [25^{th},75^{th} percentile] = -3.25, [-16.43, 5.77]; p = .47, N_{left} = 16; Right: median, [25^{th},75^{th} percentile] = 19.05, [-6.11, 36.74]; p = 0.06, Wilcoxon Sign-rank test, N_{right} = 25). This trend is difficult to interpret, as the number of stimulating electrodes differs between hemispheres, with a bias towards the right MTL (see Table 4.3 and 4.4), particularly for the spatially-oriented tasks, face-name associative memory and spatial memory. Future studies will be better able to evaluate lateralization of stimulation effects on different types of memory.

4.3.3 Stimulation type (macro vs. micro) has no effect on memory

Similarly, there was no statistically significant difference between memory performance scores for micro- and macro-stimulation (Figure 4.11; p = .08, Z = 1.76, Two-sided non-parametric Wilcoxon Rank-sum test) and no effect of micro- or macro-stimulation on memory performance, calculated separately, but there was a trend toward macro-stimulation improving performance (Macro: median, [25^{th},75^{th} percentile] = 17.50, -6.77, 68.58); p = .10, N_{macro} = 20; Micro: median, [25^{th},75^{th} percentile] = 0.00, [-16.04, 19.59]; p = 1.0, Wilcoxon Sign-rank test, N_{micro} = 21). To determine whether there was a bias in electrode placement (white/gray matter) by either stimulation type (macro/micro) or hemispheric location (left-/right), we applied two separate Chi-Square Tests of Independence to the data. There was no significant relationship between either set of variables (white/gray, micro/macro, ($\chi^2(1)$

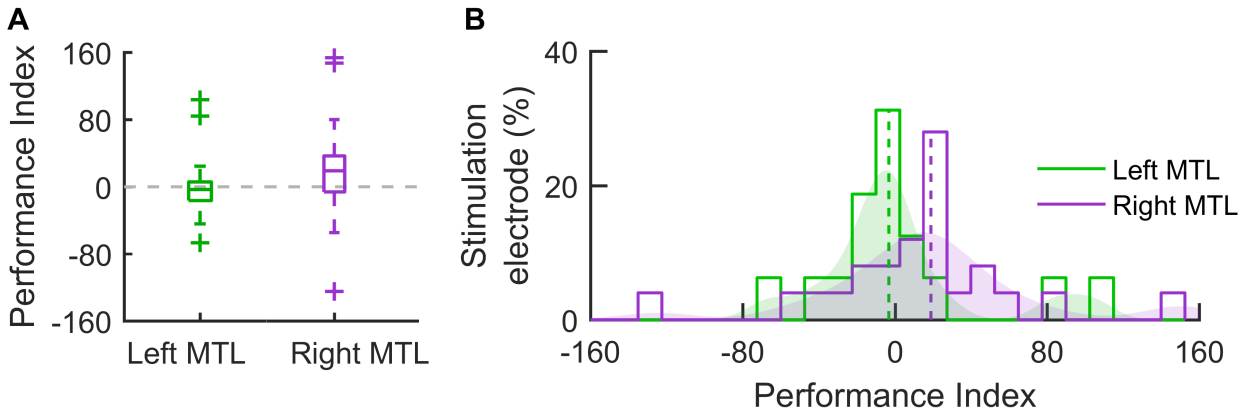

Figure 4.10: Distributions of performance index, divided by stimulated cerebral hemisphere

(A) There was no statistically significant difference in memory performance index for items that were given left medial temporal stimulation (green) and items that were given right medial temporal stimulation (purple) during learning. (B) Shown are the distributions of memory performance index scores for each individual electrode, divided by whether they were located in the left (green) or right (purple) medial temporal lobe.

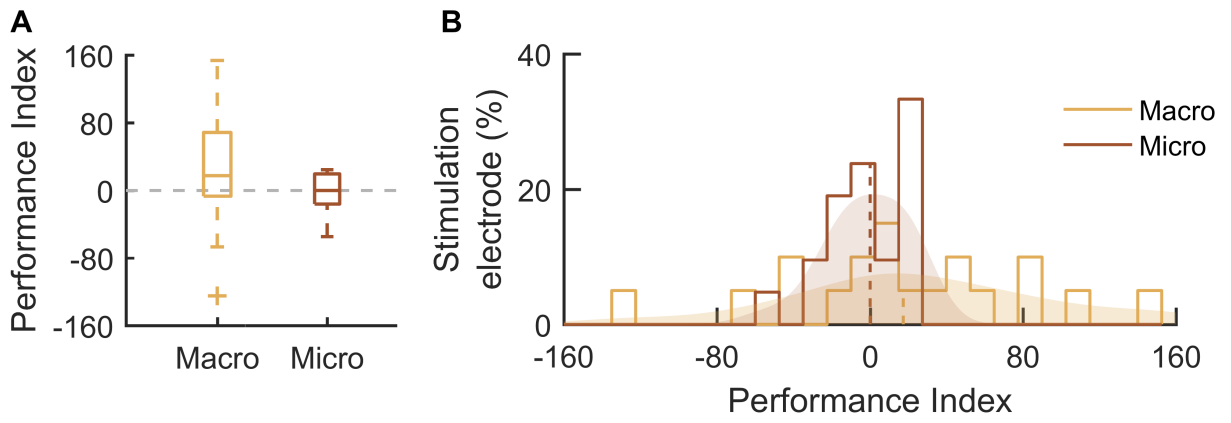

Figure 4.11: Distributions of performance index, divided by type of stimulating electrode

(A) There was no statistically significant difference in memory performance index for items that were given macro-stimulation (yellow) and items that were given micro-stimulation (brown) during learning. (B) Shown are the distributions of memory performance index scores for each individual electrode region, divided by whether they were given macro- or micro-stimulation.

= 2.97, p = .085; white/gray, left/right, $\chi^2(1) = .266$, p = .606, Chi-Square Test of Independence). Overall, these results support our finding that the divergent effects of stimulation are due to location of stimulating electrodes in entorhinal white matter vs. nearby gray matter areas, rather than the side or type of stimulation involved.

We separately recalculated two follow up ordinary least squares linear regression tests, first using only the subset of electrodes that were placed outside of the clinically-determined epileptogenic zones, and again, using the full data set but replacing the behavioral measure "discrimination index" with "fraction recollected" ("n Recollected" — "n Trials") for the object and face recognition tasks. Both tests yielded statistically similar results to the first (Table 4.2). A Bonferroni correction was applied to our alpha level as a result of running multiple linear regression tests on the same data, so coefficients were considered significant at a level of $\alpha = 0.05$, when p < .0167 (that is α/n, where n is the number of tests performed); however, stimulation of white vs. gray matter was the only statistically significant predictor

of performance index, regardless of whether the Bonferroni correction was applied or not.

4.4 Discussion

Our results demonstrate that precise targeting of DBS to entorhinal white matter in humans during learning improves hippocampal-dependent memory across a range of tasks. In contrast, stimulation of nearby gray matter is ineffective in improving MTL memory function. Thus, stimulation sites that differ by mere millimeters can have quite distinctive effects on memory.

Earlier studies of intracranial MTL stimulation in humans have yielded mixed results. A few of these studies, involving electrical stimulation of MTL gray matter, showed a disruptive [71, 72, 77, 78] or no effect on memory [14]. Other studies involving electrical stimulation of the fornix white matter showed memory enhancement [79,80] and an increase in both glucose metabolism and source-localized scalp EEG activation of the temporal lobes [81], suggesting that stimulation of hippocampal white matter afferents may have a beneficial effect. The results here also suggest that our previous finding of enhanced spatial memory by stimulation of the entorhinal region during learning [14] may be due to activation of white matter inputs to the hippocampus.

Though the specific mechanisms contributing to this memory effect remain unclear, previous rodent studies have shown that stimulation of the perforant path can potentiate neural mechanisms of learning and memory [8–13]. Recent imaging studies in humans confirmed that perforant pathway fibers are quite densely bundled within an area similar to our localized entorhinal white matter electrodes, from which they divide and disperse to various hippocampal subregions [82, 83]. By focusing stimulation on this region, these fibers can be best targeted; Conversely, adjacent gray matter stimulation may have a neutral or disruptive effect on encoding, either affecting fewer perforant fibers or introducing an overwhelming amount of noise to regions thought responsible for containing the sparsely-encoded memory trace [1, 2, 84].

One strength of the present study was the use of multiple tasks to measure declarative memory. Given the critical role of the hippocampus in declarative memory across domains, our procedure provides evidence for the generality of the benefits of entorhinal white matter stimulation. However, learning of different types of information may be differentially improved depending on the location of the stimulating electrode in entorhinal white matter. Several previous studies suggest that processing of spatial and non-spatial information relies on different MTL cortical subregions and hemispheres [85–88]. Thus, characterization of the effects of stimulation at anterior vs. posterior and left vs. right MTL structures during spatial and non-spatial memory tasks will be an important focus for future large-sample studies. Yet another question for future studies is whether DBS is more effectively applied bilaterally than unilaterally. Some studies have shown significant memory effects with bilateral stimulation [68, 79]; however, the present study confirms our previous findings [14] that unilateral stimulation may be sufficient to modulate memory. The efficacy of unilateral vs. bilateral stimulation has yet to be tested directly. Finally, the effect of stimulation type (macro vs. micro) approached significance in our results, with macro-stimulation trending towards having a greater effect on memory performance than micro-stimulation, so this distinction merits further investigation.

Recent results from clinical DBS studies, aimed at treating essential tremor and depression, emphasize the importance of electrode placement for maximal therapeutic efficacy [88, 89]. Since gray and white matter regions within the human MTL are so close in proximity (i.e., within millimeters), neuroimaging, using combined high-resolution magnetic resonance imaging and high-resolution DTI methods to improve electrode localization, will likely be optimal for targeting or analysis in future studies. Altogether, our findings suggest that, in humans, direct DBS manipulation of entorhinal white matter, not adjacent gray matter, offers a unique opportunity to improve learning and memory performance with clinical relevance to the development of therapeutic treatments for severe and debilitating memory disorders.

Subj.	Macro-stimulation Left Entorhinal		Macro-stimulation Right Entorhinal		Micro-stimulation Left Entorhinal		Micro-stimulation Right Entorhinal		
	W	**G**	**W**	**G**	**W**	**G**	**W**	**G**	**Seizure Onset Area**
1				X					Left Medial Temporal
2			X						Extra-Temporal
3			X						Left Medial Temporal
4		X		X					Left Medial Temporal
5			X						Left Lateral Temporal
6	X								Left Lateral Frontal
7		X	X						Extra-Temporal
8							X		Left Medial Temporal
9							X		Unknown
10				X			X		Bilateral Temporal
11		X		X	X			X	Extra-Temporal
12		X		X			X		Right Medial Temporal

Table 4.3: Stimulation types across subjects 1 - 12

Shown are white (W) or gray (G) matter placements of entorhinal depth macro- and micro-electrodes for all subjects and epileptogenic onset areas determined by clinical evaluation. A red X denotes an electrode that fell within an area that was later determined to be epileptogenic. To determine whether there was a bias in electrode placement (white/gray matter) by either stimulation type (macro/micro) or hemispheric location (left/right), we applied two separate Chi-Square Tests of Independence to the data

Subject	Macro-stimulation Left Entorhinal		Macro-stimulation Right Entorhinal		Micro-stimulation Left Entorhinal		Micro-stimulation Right Entorhinal		
	W	**G**	**W**	**G**	**W**	**G**	**W**	**G**	**Seizure Onset Area**
13				X		X	X		Left Medial Temporal
14		X	X		X				Unknown
15					X				Right Medial Temporal
16						X			Extra-Temporal
17						X		X	Right Medial Temporal
18								X	Right Medial Temporal
19					X		X		Left Medial Temporal
20			X				X		Extra-Temporal
21		X				X			Extra-Temporal
22							X		Left Anterior Temporal
23						X			Unknown
24				X			X		L/R Medial Temporal

Table 4.4: Stimulation types across subjects 13 - 24

Shown are white (W) or gray (G) matter placements of entorhinal depth macro- and micro-electrodes for all subjects and epileptogenic onset areas determined by clinical evaluation. A red X denotes an electrode that fell within an area that was later determined to be epileptogenic. To determine whether there was a bias in electrode placement (white/gray matter) by either stimulation type (macro/micro) or hemispheric location (left/right), we applied two separate Chi-Square Tests of Independence to the data

Neuropsychiatric scores of participants 1-12						
Subject No.	Verbal IQ *Standard Score*	Digit Span *Percentile*	Verbal Memory *WMS Percentile*	Verbal Memory *CVLT Percentile*	Visual Memory *Percentile*	Executive Function *Percentile*
1	102	91	84	84	24	90
2	-	2	25	1	1	1
3	77	16	5	16	1	1
4	81	16	1	2	1	58
5	113	75	50	69	63	6
6	103	21	84	69	34	27
7	109	25.3	15.9	29.7	4.2	2.3
8	112	91	37	1	<1	75
9	98	91	63	49	50	32
10	90[a]	16	63[b]	21[c]	<1	27
11	108	16	50	69	2	46
12	98	16	63	1	5	5

Table 4.5: Clinical Characteristics,subjects 1-12.

Verbal and digit span (i.e., attention) were calculated with the use of the Wechsler Adult Intelligence Scale, verbal memory by means of the logical memory portion of the Wechsler Memory Scale (WMS) and the long-delay free-recall portion of the California Verbal Learning Test (CVLT), visual memory with the use of the 30-second delayed version of the Rey–Osterrieth Complex Figure Test 7, and executive function by means of the Trail Making Test, Part B 30. a Full Scale IQ; b Verbal Paired Associates Delayed Recall; c Rey Auditory Verbal Learning Test score; d Above average, no score; e Spanish Neuropsychological Exam Equivalent Version.

Neuropsychiatric scores of participants 13-24						
Subject No.	Verbal IQ *Standard Score*	Digit Span *Percentile*	Verbal Memory *WMS Percentile*	Verbal Memory *CVLT Percentile*	Visual Memory *Percentile*	Executive Function *Percentile*
13	85	47	25	<1[c]	<1	<1
14	108	14	73	84	-	84
15	99	8.1	1.1	68	<1	63
16	105	37	63	50	7	63
17	125	37	63	50	96	>50[d]
18	114	37	16[b]	7	9	16
19	102	16	47	42	53	63
20	83	<1	61	8	22	-
21	105	21.1	21.2	84.1	18	0.1
22	95	9	16	2	8	21
23	105	42	16	7	8	24
24	105	99.9	5	2	<2	87

Table 4.6: Clinical Characteristics, subjects 13-24.

Verbal and digit span (i.e., attention) were calculated with the use of the Wechsler Adult Intelligence Scale, verbal memory by means of the logical memory portion of the Wechsler Memory Scale (WMS) and the long-delay free-recall portion of the California Verbal Learning Test (CVLT), visual memory with the use of the 30-second delayed version of the Rey–Osterrieth Complex Figure Test 7, and executive function by means of the Trail Making Test, Part B 30. a Full Scale IQ; b Verbal Paired Associates Delayed Recall; c Rey Auditory Verbal Learning Test score; d Above average, no score; e Spanish Neuropsychological Exam Equivalent Version.

Subject	Electrode Label	Electrode Type	Localization (Contact 1)	Localization (Contact 2)
1	REC	Macro	CA1	CA1
4	REC	Macro	Perirhinal Cortex	Fusiform Gyrus
4	LEC	Macro	Perirhinal Cortex	Perirhinal Cortex
7	LEC	Macro	Entorhinal Cortex	Perirhinal Cortex
10	REC	Macro	Perirhinal Cortex	Perirhinal Cortex
11	REC	Micro	Entorhinal Cortex	N/A
11	LEC	Macro	Perirhinal Cortex	Perirhinal Cortex
11	REC	Macro	Perirhinal Cortex	Fusiform Gyrus
12	REC	Macro	Perirhinal Cortex	Fusiform Gyrus
12	LEC	Macro	Perirhinal Cortex	Fusiform Gyrus
13	REC	Macro	Hippocampus (Subiculum)	Hippocampus (Subiculum)
13	LEC	Micro	Entorhinal Cortex	N/A
14	LEC	Macro	Perirhinal Cortex	Perirhinal Cortex
16	LEC	Micro	Entorhinal Cortex	N/A
17	REC	Micro	Entorhinal Cortex	N/A
17	LEC	Micro	Entorhinal Cortex	N/A
18	REC	Micro	Hippocampus (Subiculum)	N/A
21	LEC	Micro	Entorhinal Cortex	N/A
21	LEC	Macro	Perirhinal Cortex	Perirhinal Cortex
23	LEC	Micro	Entorhinal Cortex	N/A
24	REC	Macro	Perirhinal Cortex	Perirhinal Cortex

Table 4.7: Electrode localizations

Shown are gray matter electrode localizations of subjects with the 15 micro- or macro-electrodes that fell within medial temporal subregions. Electrode labels include right and left entorhinal cortices (REC,LEC). For each stimulated macro-electrode pair (contact 1 is more distal than contact 2) or micro-electrode, contacts were actually localized to entorhinal cortex (more inferior medial placements), perirhinal cortex (more lateral inferior placement), or hippocampal subiculum (more superior placement). Micro-electrode contacts (both stimulating and reference electrode) are localized to the same region (contact 1) and therefore localization of contact 2 is not applicable (N/A).

References

[1] H. Eichenbaum, "A cortical-hippocampal system for declarative memory," *Nat. Rev. Neurosci.*, vol. 1, pp. 41–50, Oct 2000.

[2] L. R. Squire, C. E. Stark, and R. E. Clark, "The medial temporal lobe," *Annu. Rev. Neurosci.*, vol. 27, pp. 279–306, 2004.

[3] L. L. Colgin and E. I. Moser, "Hippocampal theta rhythms follow the beat of their own drum," *Nat. Neurosci.*, vol. 12, pp. 1483–1484, Dec 2009.

[4] L. L. Colgin, "Theta-gamma coupling in the entorhinal-hippocampal system," *Curr. Opin. Neurobiol.*, vol. 31, pp. 45–50, Apr 2015.

[5] A. B. Tort, R. W. Komorowski, J. R. Manns, N. J. Kopell, and H. Eichenbaum, "Theta-gamma coupling increases during the learning of item-context associations," *Proc. Natl. Acad. Sci. U.S.A.*, vol. 106, pp. 20942–20947, Dec 2009. [PubMed Central:PMC2791641] [DOI:10.1073/pnas.0911331106] [PubMed:19934062].

[6] K. M. Igarashi, L. Lu, L. L. Colgin, M. B. Moser, and E. I. Moser, "Coordination of entorhinal-hippocampal ensemble activity during associative learning," *Nature*, vol. 510, pp. 143–147, Jun 2014.

[7] E. W. Schomburg, A. Fernandez-Ruiz, K. Mizuseki, A. Berenyi, C. A. Anastassiou, C. Koch, and G. Buzsaki, "Theta phase segregation of input-specific gamma patterns in entorhinal-hippocampal networks," *Neuron*, vol. 84, pp. 470–485, Oct 2014.

[8] E. Pastalkova, P. Serrano, D. Pinkhasova, E. Wallace, A. A. Fenton, and T. C. Sacktor, "Storage of spatial information by the maintenance mechanism of LTP," *Science*, vol. 313, pp. 1141–1144, Aug 2006.

[9] A. Ehret, A. Haaf, H. Jeltsch, B. Heimrich, T. J. Feuerstein, and R. Jackisch, "Modulation of electrically evoked acetylcholine release in cultured rat septal neurones," *J. Neurochem.*, vol. 76, pp. 555–564, Jan 2001.

[10] T. J. Feuerstein and W. Seeger, "Modulation of acetylcholine release in human cortical slices: possible implications for Alzheimer's disease," *Pharmacol. Ther.*, vol. 74, no. 3, pp. 333–347, 1997. [PubMed:9352588].

[11] R. P. Vertes, "Hippocampal theta rhythm: a tag for short-term memory," *Hippocampus*, vol. 15, no. 7, pp. 923–935, 2005.

[12] J. M. Williams and B. Givens, "Stimulation-induced reset of hippocampal theta in the freely performing rat," *Hippocampus*, vol. 13, no. 1, pp. 109–116, 2003.

[13] D. S. Roy, A. Arons, T. I. Mitchell, M. Pignatelli, T. J. Ryan, and S. Tonegawa, "Memory retrieval by activating engram cells in mouse models of early Alzheimer's disease," *Nature*, vol. 531, pp. 508–512, Mar 2016.

[14] N. Suthana, Z. Haneef, J. Stern, R. Mukamel, E. Behnke, B. Knowlton, and I. Fried, "Memory enhancement and deep-brain stimulation of the entorhinal area," *N. Engl. J. Med.*, vol. 366, pp. 502–510, Feb 2012.

[15] L. L. Colgin, T. Denninger, M. Fyhn, T. Hafting, T. Bonnevie, O. Jensen, M. B. Moser, and E. I. Moser, "Frequency of gamma oscillations routes flow of information in the hippocampus," *Nature*, vol. 462, pp. 353–357, Nov 2009.

[16] F. Mormann, J. Fell, N. Axmacher, B. Weber, K. Lehnertz, C. E. Elger, and G. Fernandez, "Phase/amplitude reset and theta-gamma interaction in the human medial temporal lobe during a continuous word recognition memory task," *Hippocampus*, vol. 15, no. 7, pp. 890–900, 2005.

[17] M. F. Carr, M. P. Karlsson, and L. M. Frank, "Transient slow gamma synchrony underlies hippocampal memory replay," *Neuron*, vol. 75, pp. 700–713, Aug 2012.

[18] K. W. Bieri, K. N. Bobbitt, and L. L. Colgin, "Slow and fast $\hat{\text{I}}^3$ rhythms coordinate different spatial coding modes in hippocampal place cells," *Neuron*, vol. 82, pp. 670–681, May 2014.

[19] J. Yamamoto, J. Suh, D. Takeuchi, and S. Tonegawa, "Successful execution of working memory linked to synchronized high-frequency gamma oscillations," *Cell*, vol. 157, pp. 845–857, May 2014.

[20] C. Zheng, K. Wood Bieri, E. Hwaun, and L. Lee Colgin, "Fast Gamma Rhythms in the Hippocampus Promote Encoding of Novel Object-Place Pairings," *eNeuro*, vol. 3, no. 2, 2016.

[21] B. Lega, J. Burke, J. Jacobs, and M. J. Kahana, "Slow-Theta-to-Gamma Phase-Amplitude Coupling in Human Hippocampus Supports the Formation of New Episodic Memories," *Cereb. Cortex*, vol. 26, pp. 268–278, Jan 2016.

[22] H. O. Cabral, M. Vinck, C. Fouquet, C. M. Pennartz, L. Rondi-Reig, and F. P. Battaglia, "Oscillatory dynamics and place field maps reflect hippocampal ensemble processing of sequence and place memory under NMDA receptor control," *Neuron*, vol. 81, pp. 402–415, Jan 2014.

[23] K. M. JE Meyers, *Rey complex figure test and recognition trial: Professional manual.* Odessa,FL, 1995.

[24] R. Reitan, *Trail Making Test: Manual for administration and scoring*, 1992.

[25] Delis,D.C. and Kramer, J.H. and Kaplan, E. and Ober, B.A, *California Verbal Learning Test.* San Antonio, TX., 2000.

[26] Wechsler,D., *Wechsler Memory Scale, revised.* New York, 2005.

[27] Wechsler,D., *Wechsler Adult Intelligence Scale.* San Antonio, TX.

[28] D. H. Brainard, "The Psychophysics Toolbox," *Spat Vis*, vol. 10, no. 4, pp. 433–436, 1997.

[29] I. Fried, C. L. Wilson, J. Zhang, *et al.*, "Implantation of depth electrodes for EEG recording.," in *Stereotactic surgery and radiosurgery.* (A. De Salles and S. Goetsch, eds.), (Madison,WI.), pp. 149–158, Medical Physics Publishing., 1993.

[30] I. Fried, K. A. MacDonald, and C. L. Wilson, "Single neuron activity in human hippocampus and amygdala during recognition of faces and objects," *Neuron*, vol. 18, pp. 753–765, May 1997.

[31] I. Fried, C. L. Wilson, N. T. Maidment, J. Engel, E. Behnke, T. A. Fields, K. A. MacDonald, J. W. Morrow, and L. Ackerson, "Cerebral microdialysis combined with single-neuron and electroencephalographic recording in neurosurgical patients. Technical note," *J. Neurosurg.*, vol. 91, pp. 697–705, Oct 1999.

[32] R. Q. Quiroga, Z. Nadasdy, and Y. Ben-Shaul, "Unsupervised spike detection and sorting with wavelets and superparamagnetic clustering," *Neural Comput*, vol. 16, pp. 1661–1687, Aug 2004.

[33] R. Q. Quiroga, L. Reddy, G. Kreiman, C. Koch, and I. Fried, "Invariant visual representation by single neurons in the human brain," *Nature*, vol. 435, pp. 1102–1107, Jun 2005.

[34] *Neuroport Bio-potential Signal Processing System, User's Manual, Revision 4.00.* salt Lake City, UT, 2011.

[35] H. K. Gumprecht, D. C. Widenka, and C. B. Lumenta, "BrainLab VectorVision Neuronavigation System: technology and clinical experiences in 131 cases," *Neurosurgery*, vol. 44, pp. 97–104, Jan 1999.

[36] J. R. Schlaier, J. Warnat, U. Dorenbeck, M. Proescholdt, K. M. Schebesch, and A. Brawanski, "Image fusion of MR images and real-time ultrasonography: evaluation of fusion accuracy combining two commercial instruments, a neuronavigation system and a ultrasound system," *Acta Neurochir (Wien)*, vol. 146, pp. 271–276, Mar 2004.

[37] M. Jenkinson and S. Smith, "A global optimisation method for robust affine registration of brain images," *Med Image Anal*, vol. 5, pp. 143–156, Jun 2001.

[38] M. Jenkinson, P. Bannister, M. Brady, and S. Smith, "Improved optimization for the robust and accurate linear registration and motion correction of brain images," *Neuroimage*, vol. 17, pp. 825–841, Oct 2002.

[39] J. Pluta, P. Yushkevich, S. Das, and D. Wolk, "In vivo analysis of hippocampal subfield atrophy in mild cognitive impairment via semi-automatic segmentation of T2-weighted MRI," *J. Alzheimers Dis.*, vol. 31, no. 1, pp. 85–99, 2012.

[40] P. A. Yushkevich, H. Wang, J. Pluta, S. R. Das, C. Craige, B. B. Avants, M. W. Weiner, and S. Mueller, "Nearly automatic segmentation of hippocampal subfields in in vivo focal T2-weighted MRI," *Neuroimage*, vol. 53, pp. 1208–1224, Dec 2010.

[41] D. Amaral and R. Insausti, *The Human Nervous System (v. 1)*. Academic Press, 1990.

[42] H. M. Duvernoy, F. Cattin, and P.-Y. Risold, *The Human Hippocampus: Functional Anatomy, Vascularization and Serial Sections with MRI*. Springer, 2013.

[43] Y. Zhang, M. Brady, and S. Smith, "Segmentation of brain MR images through a hidden Markov random field model and the expectation-maximization algorithm," *IEEE Trans Med Imaging*, vol. 20, pp. 45–57, Jan 2001.

[44] N. A. Suthana, A. D. Ekstrom, S. Moshirvaziri, B. Knowlton, and S. Y. Bookheimer, "Human hippocampal CA1 involvement during allocentric encoding of spatial information," *J. Neurosci.*, vol. 29, pp. 10512–10519, Aug 2009.

[45] A. Ekstrom, N. Suthana, E. Behnke, N. Salamon, S. Bookheimer, and I. Fried, "High-resolution depth electrode localization and imaging in patients with pharmacologically intractable epilepsy," *J. Neurosurg.*, vol. 108, pp. 812–815, Apr 2008.

[46] M. M. Zeineh, S. A. Engel, P. M. Thompson, and S. Y. Bookheimer, "Dynamics of the hippocampus during encoding and retrieval of face-name pairs," *Science*, vol. 299, pp. 577–580, Jan 2003.

[47] A. Delorme and S. Makeig, "EEGLAB: an open source toolbox for analysis of single-trial EEG dynamics including independent component analysis," *J. Neurosci. Methods*, vol. 134, pp. 9–21, Mar 2004.

[48] R. T. Canolty, E. Edwards, S. S. Dalal, M. Soltani, S. S. Nagarajan, H. E. Kirsch, M. S. Berger, N. M. Barbaro, and R. T. Knight, "High gamma power is phase-locked to theta oscillations in human neocortex," *Science*, vol. 313, pp. 1626–1628, Sep 2006.

[49] H. JW and H. JM, *Generalized Estimating Equations*. CRC Press, 2005.

[50] E. Tulving, "On the law of primacy.," in *Memory and Mind:A Festschrift for Gordon H. Bower.* (K. S. Gluck MA, Anderson JR, ed.), (NJ), pp. 31–48, Lawrence Erlbaum Associates., 2007.

[51] M. B. Merkow, J. F. Burke, J. M. Stein, and M. J. Kahana, "Prestimulus theta in the human hippocampus predicts subsequent recognition but not recall," *Hippocampus*, vol. 24, pp. 1562–1569, Dec 2014.

[52] P. Fries, "A mechanism for cognitive dynamics: neuronal communication through neuronal coherence," *Trends Cogn. Sci. (Regul. Ed.)*, vol. 9, pp. 474–480, Oct 2005.

[53] G. Buzsaki, "Theta rhythm of navigation: link between path integration and landmark navigation, episodic and semantic memory," *Hippocampus*, vol. 15, no. 7, pp. 827–840, 2005.

[54] M. J. Kahana, D. Seelig, and J. R. Madsen, "Theta returns," *Curr. Opin. Neurobiol.*, vol. 11, pp. 739–744, Dec 2001. [PubMed:11741027].

[55] J. Jacobs, M. J. Kahana, A. D. Ekstrom, M. V. Mollison, and I. Fried, "A sense of direction in human entorhinal cortex," *Proc. Natl. Acad. Sci. U.S.A.*, vol. 107, pp. 6487–6492, Apr 2010.

[56] B. C. Lega, J. Jacobs, and M. Kahana, "Human hippocampal theta oscillations and the formation of episodic memories," *Hippocampus*, vol. 22, pp. 748–761, Apr 2012.

[57] S. Guderian, B. H. Schott, A. Richardson-Klavehn, and E. Duzel, "Medial temporal theta state before an event predicts episodic encoding success in humans," *Proc. Natl. Acad. Sci. U.S.A.*, vol. 106, pp. 5365–5370, Mar 2009.

[58] O. S. Vinogradova, E. S. Brazhnik, V. F. Kichigina, and V. S. Stafekhina, "Modulation of the reaction of hippocampal neurons to sensory stimuli by cholinergic substances," *Neurosci. Behav. Physiol.*, vol. 26, no. 2, pp. 113–124, 1996.

[59] H. McCartney, A. D. Johnson, Z. M. Weil, and B. Givens, "Theta reset produces optimal conditions for long-term potentiation," *Hippocampus*, vol. 14, no. 6, pp. 684–687, 2004.

[60] C. D. Tesche and J. Karhu, "Theta oscillations index human hippocampal activation during a working memory task," *Proc. Natl. Acad. Sci. U.S.A.*, vol. 97, pp. 919–924, Jan 2000.

[61] D. S. Rizzuto, J. R. Madsen, E. B. Bromfield, A. Schulze-Bonhage, D. Seelig, R. Aschenbrenner-Scheibe, and M. J. Kahana, "Reset of human neocortical oscillations during a working memory task," *Proc. Natl. Acad. Sci. U.S.A.*, vol. 100, pp. 7931–7936, Jun 2003.

[62] R. T. Canolty and R. T. Knight, "The functional role of cross-frequency coupling," *Trends Cogn. Sci. (Regul. Ed.)*, vol. 14, pp. 506–515, Nov 2010.

[63] W. F. Agnew and D. B. McCreery, "Considerations for safety with chronically implanted nerve electrodes," *Epilepsia*, vol. 31 Suppl 2, pp. 27–32, 1990.

[64] B. Gordon, R. P. Lesser, N. E. Rance, J. Hart, R. Webber, S. Uematsu, and R. S. Fisher, "Parameters for direct cortical electrical stimulation in the human: histopathologic confirmation," *Electroencephalogr Clin Neurophysiol*, vol. 75, pp. 371–377, May 1990.

[65] P. Boon, K. Vonck, V. De Herdt, A. Van Dycke, M. Goethals, L. Goossens, M. Van Zandijcke, T. De Smedt, I. Dewaele, R. Achten, W. Wadman, F. Dewaele, J. Caemaert, and D. Van Roost, "Deep brain stimulation in patients with refractory temporal lobe epilepsy," *Epilepsia*, vol. 48, pp. 1551–1560, Aug 2007.

[66] B. Jobst, "Brain stimulation for surgical epilepsy," *Epilepsy Res.*, vol. 89, pp. 154–161, Mar 2010.

[67] J. Jacobs, "Hippocampal theta oscillations are slower in humans than in rodents: implications for models of spatial navigation and memory," *Philos. Trans. R. Soc. Lond., B, Biol. Sci.*, vol. 369, p. 20130304, Feb 2014.

[68] S. S. Stone, C. M. Teixeira, L. M. Devito, K. Zaslavsky, S. A. Josselyn, A. M. Lozano, and P. W. Frankland, "Stimulation of entorhinal cortex promotes adult neurogenesis and facilitates spatial memory," *J. Neurosci.*, vol. 31, pp. 13469–13484, Sep 2011.

[69] H. Toda, C. Hamani, A. P. Fawcett, W. D. Hutchison, and A. M. Lozano, "The regulation of adult rodent hippocampal neurogenesis by deep brain stimulation," *J. Neurosurg.*, vol. 108, pp. 132–138, Jan 2008.

[70] J. C. Augustinack, K. Helmer, K. E. Huber, S. Kakunoori, L. Zollei, and B. Fischl, "Direct visualization of the perforant pathway in the human brain with ex vivo diffusion tensor imaging," *Front Hum Neurosci*, vol. 4, p. 42, 2010.

[71] E. Halgren and C. L. Wilson, "Recall deficits produced by afterdischarges in the human hippocampal formation and amygdala," *Electroencephalogr Clin Neurophysiol*, vol. 61, pp. 375–380, Nov 1985.

[72] E. Halgren, C. L. Wilson, and J. M. Stapleton, "Human medial temporal-lobe stimulation disrupts both formation and retrieval of recent memories," *Brain Cogn*, vol. 4, pp. 287–295, Jul 1985.

[73] D. R. Merrill, M. Bikson, and J. G. Jefferys, "Electrical stimulation of excitable tissue: design of efficacious and safe protocols," *J. Neurosci. Methods*, vol. 141, pp. 171–198, Feb 2005.

[74] M. P. Toglia, "Withstanding the test of time: the 1978 semantic word norms," *Behav Res Methods*, vol. 41, pp. 531–533, May 2009.

[75] T. F. Brady, T. Konkle, G. A. Alvarez, and A. Oliva, "Visual long-term memory has a massive storage capacity for object details," *Proc. Natl. Acad. Sci. U.S.A.*, vol. 105, pp. 14325–14329, Sep 2008.

[76] N. A. Suthana, N. N. Parikshak, A. D. Ekstrom, M. J. Ison, B. J. Knowlton, S. Y. Bookheimer, and I. Fried, "Specific responses of human hippocampal neurons are associated with better memory," *Proc. Natl. Acad. Sci. U.S.A.*, vol. 112, pp. 10503–10508, Aug 2015.

[77] S. G. Coleshill, C. D. Binnie, R. G. Morris, G. Alarcon, W. van Emde Boas, D. N. Velis, A. Simmons, C. E. Polkey, C. W. van Veelen, and P. C. van Rijen, "Material-specific recognition memory deficits elicited by unilateral hippocampal electrical stimulation," *J. Neurosci.*, vol. 24, pp. 1612–1616, Feb 2004.

[78] M. E. Lacruz, A. Valentin, J. J. Seoane, R. G. Morris, R. P. Selway, and G. Alarcon, "Single pulse electrical stimulation of the hippocampus is sufficient to impair human episodic memory," *Neuroscience*, vol. 170, pp. 623–632, Oct 2010.

[79] C. Hamani, M. P. McAndrews, M. Cohn, M. Oh, D. Zumsteg, C. M. Shapiro, R. A. Wennberg, and A. M. Lozano, "Memory enhancement induced by hypothalamic/fornix deep brain stimulation," *Ann. Neurol.*, vol. 63, pp. 119–123, Jan 2008.

[80] J. P. Miller, J. A. Sweet, C. M. Bailey, C. N. Munyon, H. O. Luders, and P. S. Fastenau, "Visual-spatial memory may be enhanced with theta burst deep brain stimulation of the fornix: a preliminary investigation with four cases," *Brain*, vol. 138, pp. 1833–1842, Jul 2015.

[81] A. W. Laxton, D. F. Tang-Wai, M. P. McAndrews, D. Zumsteg, R. Wennberg, R. Keren, J. Wherrett, G. Naglie, C. Hamani, G. S. Smith, and A. M. Lozano, "A phase I trial of deep brain stimulation of memory circuits in Alzheimer's disease," *Ann. Neurol.*, vol. 68, pp. 521–534, Oct 2010.

[82] M. M. Zeineh, N. Palomero-Gallagher, M. Axer, D. Gra?el, M. Goubran, A. Wree, R. Woods, K. Amunts, and K. Zilles, "Direct Visualization and Mapping of the Spatial Course of Fiber Tracts at Microscopic Resolution in the Human Hippocampus," *Cereb. Cortex*, Feb 2016.

[83] M. A. Yassa, L. T. Muftuler, and C. E. Stark, "Ultrahigh-resolution microstructural diffusion tensor imaging reveals perforant path degradation in aged humans in vivo," *Proc. Natl. Acad. Sci. U.S.A.*, vol. 107, pp. 12687–12691, Jul 2010.

[84] F. Girgis and J. P. Miller, "White matter stimulation for the treatment of epilepsy," *Seizure*, vol. 37, pp. 28–31, Apr 2016.

[85] W. A. Suzuki and D. G. Amaral, "Perirhinal and parahippocampal cortices of the macaque monkey: cortical afferents," *J. Comp. Neurol.*, vol. 350, pp. 497–533, Dec 1994.

[86] V. Frisk and B. Milner, "The relationship of working memory to the immediate recall of stories following unilateral temporal or frontal lobectomy," *Neuropsychologia*, vol. 28, no. 2, pp. 121–135, 1990.

[87] M. L. Smith and B. Milner, "Right hippocampal impairment in the recall of spatial location: encoding deficit or rapid forgetting?," *Neuropsychologia*, vol. 27, no. 1, pp. 71–81, 1989.

[88] N. Pouratian, Z. Zheng, A. A. Bari, E. Behnke, W. J. Elias, and A. A. Desalles, "Multi-institutional evaluation of deep brain stimulation targeting using probabilistic connectivity-based thalamic segmentation," *J. Neurosurg.*, vol. 115, pp. 995–1004, Nov 2011.

[89] Riva-Posse, P. and Choi, K. S. and Holtzheimer, P. E. and McIntyre, C. C. and Gross, R. E. and Chaturvedi, A. and Crowell, A. L. and Garlow, S. J. and Rajendra, J. K. and Mayberg, H. S. , "Defining critical white matter pathways mediating successful subcallosal cingulate deep brain stimulation for treatment-resistant depression," *Biol. Psychiatry*, vol. 76, pp. 963–969, Dec 2014.